

I-type granitoids in the eastern Yangtze Block: implications for the Early Paleozoic intracontinental orogeny in South China



Yili Guan^{a,b}, Chao Yuan^{a,*}, Min Sun^c, Simon Wilde^d, Xiaoping Long^a, Xiaolong Huang^a, Qiang Wang^a

^a State Key Laboratory of Isotope Geochemistry, Guangzhou Institute of Geochemistry, Chinese Academy of Sciences, Guangzhou 510640, Guangdong China

^b University of Chinese Academy of Sciences, Beijing 10069, China

^c Department of Earth Sciences, The University of Hong Kong, Pokfulam Road, Hong Kong

^d Department of Applied Geology, Curtin University, Perth WA 6845, Australia

ARTICLE INFO

Article history:

Received 28 December 2013

Accepted 19 July 2014

Available online 27 July 2014

Keywords:

South China

Intracontinental orogeny

Adakitic rocks

Lithosphere reworking

Delamination

ABSTRACT

The Early Paleozoic intracontinental orogenic belt in the South China Block (SCB) is composed of massive granitoids and high-grade metamorphic rocks. Compared to the widespread distributions of early Paleozoic S-type granites in the eastern SCB, coeval I-type granitoids are rare and consequently receive much less attention. Two spatially associated granodiorite plutons in the northwestern rim of the orogen, namely the Banshanpu pluton and Hongxiaqiao pluton, have been investigated in order to determine how they fit into the geodynamic setting. The Hongxiaqiao pluton shares many lithological similarities with the Banshanpu pluton, except for the presence of abundant mafic microgranular enclaves (MMEs) in the Hongxiaqiao pluton. Zircon U–Pb dating has yielded weighted mean $^{206}\text{Pb}/^{238}\text{U}$ ages of 432 ± 3 Ma and 434 ± 3 Ma for the Banshanpu and Hongxiaqiao plutons, respectively, indicating that they were emplaced coevally in the early Silurian. Samples from the two plutons possess similar Nd–Sr isotope compositions ($\epsilon\text{Nd}_T = -8.32$ to -6.88 ; $^{87}\text{Sr}/^{86}\text{Sr}_i = 0.7109$ – 0.7169), indicating that they were derived from a similar crustal source. Rocks from the Banshanpu pluton are intermediate- to high-K calc-alkaline and show strongly peraluminous ($A/\text{CNK} > 1.1$), adakite-like characteristics (Sr/Y ratios > 31 ; $\text{Yb} < 0.91$ ppm), consistent with an origin of partial melting of amphibolite in the garnet stability field. Samples from the Hongxiaqiao pluton contain lower SiO_2 but considerably higher Fe_2O_3 , TiO_2 , P_2O_5 and highly incompatible elements (e.g. Rb, Cs, Th and U) than those of the Banshanpu pluton. The MMEs from the Hongxiaqiao pluton give ages similar to that of their host granite (429 ± 5 Ma), and their Nd–Sr isotope compositions ($\epsilon\text{Nd}_T = -7.45$ to -7.03 ; $^{87}\text{Sr}/^{86}\text{Sr}_i = 0.7115$ – 0.7143) imply an origin from metasomatized lithospheric mantle. The Hongxiaqiao pluton was possibly produced by a magma mixing between a crustal melt and a lithospheric mantle-derived melt. Because the MMEs have relatively low Sr/Y (9–17) and $(\text{La}/\text{Yb})_N$ (3–15) ratios, mixing of the lithospheric mantle-derived melt with an adakite-like melt would dilute the adakitic signature and make composition of the mixture deviate from adakitic characteristics. A comprehensive evaluation of geochronological data for magmatism and metamorphism in the orogeny reveals two phases of orogenesis: one before and one after ca. 440 Ma. The temporal and spatial developments of tectonomagmatism, as well as the increase in metamorphic grade, are interpreted to record the progress of the intracontinental orogeny, which started in the Wuyi-Yunkai domains of the Cathaysia Block in the Ordovician and propagated westward into the Yangtze Block in the Silurian.

© 2014 Elsevier B.V. All rights reserved.

1. Introduction

Orogenic belts commonly form at convergent plate margins and preserve important information of continental accretion and amalgamation (Wilson, 1965). Two categories for orogenic belts have been recognized (Windley, 1995), i.e. collisional orogens formed by collision of two continents (e.g. Himalaya and Alps, Sengör et al., 1993; Yin and Harrison, 2000; Rossetti et al., 2004), and accretionary

orogens generated by accretion of juvenile materials such as sea-mounts and island-arcs (Sengör et al., 1993; Windley, 1995). Distinctly different from the conventional orogenic belts along plate margins, a third category, namely intra-continental (or intraplate) orogenic belt, has also been recognized. Orogenic belts of the third type are normally located hundreds or even thousands of kilometers away from the edge of the continent, and commonly associated with continental reactivation and reworking (Cawood and Tyler, 2004; Holdsworth et al., 2001; Sandiford and Hand, 1998). Examples include the Cenozoic Tianshan orogenic belt in Central Asia (Yin et al., 1998), the Petermann and Alice Springs orogenic belts in central Australia (Hand and Sandiford, 1999; Raimondo et al., 2010), and

* Corresponding author at: Guangzhou Institute of Geochemistry, Chinese Academy of Sciences, Kehua Street 511, Tianhe District, Guangzhou 510640, China. Tel.: +86 20 8529 0708; fax: +86 20 8529 0130.

E-mail address: yuanchao@gig.ac.cn (C. Yuan).

to evolve into an ocean, as evidenced by the lack of contemporaneous ophiolite or slices of oceanic lithosphere (Shu et al., 2011). Rift-related magmatism occurred mainly around 780–740 Ma (Wang and Li, 2003; Zheng et al., 2008), and there is no sign of magmatism after 740 Ma, although numerous 500–700 Ma magmatic detrital and inherited zircons associated with the Late Neoproterozoic–Cambrian orogen have been reported (Li et al., 2014; Yao et al., 2014). In the early Paleozoic, a compressional regime dominated the tectonic evolution of the area and gave rise to the final closure of the Nanhua rift and intracontinental orogenesis (Wang and Li, 2003), resulting in not only deformation and metamorphism of pre-Devonian rocks (Shu, 2006), but also extensive felsic magmatism (Chu et al., 2012; Y.J. Wang et al., 2011; C. Zhang et al., 2011; Zhang et al., 2012). After the intracontinental orogenic event, the SCB remained relatively intact until the early to middle Permian (X.H. Li et al., 2012), when intensive reworking of the pre-Jurassic rocks brought about widespread crustal melting and ~80% of total granitic rocks in the eastern SCB (Sun, 2006).

Both the Cathysia and Yangtze blocks were involved in the Wuyi-Yunkai Orogen. However, these two blocks show different manifestations of the intracontinental orogenesis, with the Cathysia Block having experienced more intensive metamorphism, deformation and magmatism. For example, the Wuyi-Yunkai domains in the Cathysia Block experienced both thin- and thick-skinned thrust tectonics and greenschist to granulite facies metamorphism (Fig. 1, Charvet et al., 2010; Faure et al., 2009; Z.X. Li et al., 2010), whereas the area between the Ganjiang Fault in the Cathysia Block and the Zhangjiajie-Huayuan-Kaili Fault in the Yangtze Block underwent greenschist metamorphism and only thin-skinned thrust tectonics (Charvet et al., 2010; Hu et al., 2010). The oldest stratum exposed in the study area is the Neoproterozoic Lengjiaxi Group, and recent investigation on the Lengjiaxi Group around the study area has revealed a mafic volcanic rock-dominated section, which constitutes the basement of the study area and consists of greenschist to amphibolite phase tholeiitic basalt and basaltic andesite with subordinate pelite (Wu et al., 2004). More than one hundred early Paleozoic granitic plutons are distributed between the Anhua-Luocheng Fault and the Zhenghe-Dapu Fault (Fig. 1). Most of these granitic intrusions are within the Cathysia Block, while early Paleozoic granites in the Yangtze Block are only sporadically exposed.

2.2. Early Paleozoic granitoids

Early Paleozoic felsic intrusions in the Wuyi-Yunkai Orogen are mainly peraluminous, dominated by S-type granites (Shu, 2006). The lack of mafic enclaves and their crustal Nd–Hf isotope compositions suggest that the S-type granites were mainly derived from partial melting of crustal materials. In comparison with the widely distributed S-type granites, I-type granites occur sporadically in the orogen and have not been well studied. Among Early Paleozoic I-type granitic intrusions of the Wuyi-Yunkai Orogen, two plutons in the SE Yangtze Block, i.e. the Banshanpu pluton and the Hongxiaqiao pluton (Fig. 1), are selected for further investigation. The two plutons are hornblende-bearing I-type granitoids and one exhibits strongly peraluminous, adakitic characteristics (Xu et al., 2006), which are quite unusual and only sporadically reported (e.g. Q. Wang et al., 2011). Both the Banshanpu and Hongxiaqiao plutons are round in shape and occur in close proximity, being 0.5 km apart (Fig. 2). The plutons were intruded into the Neoproterozoic Lengjiaxi Group, and are overlain by Late Paleozoic strata (BGMHRP, 1988) (Fig. 2). The plutons are undeformed, and the rocks generally show massive, medium-grained structure. Rocks of the Banshanpu pluton consist mainly of quartz (25–35 vol.%), plagioclase (30–45 vol.%), K-feldspar (15–30 vol.%), biotite (10–15 vol.%), hornblende (~5 vol.%) and accessory zircon, apatite, titanite, allanite and Fe–Ti oxide. Rocks of the Hongxiaqiao pluton have a similar mineral assemblage, with lesser proportions of quartz (20–30 vol.%) and K-feldspar (10–20 vol.%), and more abundant plagioclase (40–50 vol.%), biotite (10–20 vol.%) and hornblende (5–10 vol.%). The two plutons

have similar mineral association, whereas the Hongxiaqiao pluton has higher proportion of Fe–Ti oxide. Both plutons contain xenoliths of wall rock, mainly near the margins. Zircon and apatite are commonly seen as inclusions within hornblende and biotite, whereas titanite and allanite generally coexist with feldspar and quartz. A striking difference between the two plutons is that mafic microgranular enclaves (MMEs) commonly occur in the Hongxiaqiao pluton, but are only rarely observed in the Banshanpu pluton.

2.3. MMEs within the Hongxiaqiao pluton

Most MMEs in the Hongxiaqiao pluton are elongated to ellipsoidal in shape (Fig. 3), and are gray to dark-gray in color, with size ranging from a few to tens of centimeters. Most MMEs show sharp boundaries with their host, although some do exhibit transitional characteristics. The MMEs have a porphyritic texture, with 10–20 vol.% of phenocrysts. The matrix consists mainly of plagioclase (30–40 vol.%), hornblende (10–20 vol.%), biotite (10–20 vol.%) and, locally, quartz (<5 vol.%), with subordinate Fe–Ti oxides and acicular apatite. The megacrysts consist of K-feldspar and plagioclase with complex zoning, although quartz and biotite can locally be found. In contrast with the minerals of the host rock that are normally tabular or stubby in shape, crystals of plagioclase and hornblende in the MMEs are slender and elongated. Some megacrysts of K-feldspar, biotite and quartz in the MMEs exhibit a sieve-like texture, with tiny grains of plagioclase, hornblende and biotite being enclosed within the megacrysts.

3. Analytical methods

3.1. Zircon U–Pb isotope analyses

Zircons were separated using heavy liquid and magnetic techniques, and then purified by hand picking under a binocular microscope. About 100 grains were randomly selected and mounted on adhesive tape then enclosed in epoxy resin and polished to about half their thickness. After being photographed under reflected and transmitted light, the samples were prepared for U–Pb dating. In order to investigate the structure of the zircons and to choose target sites for U–Pb isotopic analyses, cathodoluminescence (CL) imaging was carried out using a JXA-8100 Electron Probe Microanalyzer with Mono CL3 Cathodoluminescence System for high resolution imaging and spectroscopy at the Guangzhou Institute of Geochemistry, Chinese Academy of Sciences (GIGCAS). CL images of typical zircon grains are presented in Fig. 4. Zircon U–Pb dating for the two granitic plutons (samples YLL-1 and YH-1) was carried out using an Agilent 7500a ICP-MS, coupled with a 193 nm wave laser microprobe, at the State Key Laboratory of Isotope Geochronology and Geochemistry, GIGCAS. Laser energy was 80 mJ and frequency was 10 Hz with ablation spot of 31 μm in diameter and 40 s ablation times. Zircon 91500 was used as the external standard for U–Pb dating, and was analyzed once every 5 analyses. Detailed analytical procedures were similar to those described by Li et al. (2011). Off-line selection and integration of background and analyte signals, and time-drift correction and quantitative calibration for U–Pb dating were performed using the software ICPMS DataCal 8.4 (Liu et al., 2010). Correction of common-Pb followed the method described by Andersen (2002), and the dating results are presented in the concordia diagrams (Fig. 4). ISOPLOT (version 3.0) (Ludwig, 2003) was used to plot concordia diagrams and for age calculations. Individual analyses with 1σ errors are available as supplementary online material in Appendix A, and uncertainties in age results are quoted at the 95% level (1σ).

Analyses for zircons from an MME sample (10BG2-4) were conducted using the Cameca IMS-1280 SIMS at the Institute of Geology and Geophysics, Chinese Academy of Sciences. The instrument description and analytical procedure can be found in Li et al. (2009b), and only a brief summary is described here. The primary O_2^- ion beam spot is about $20 \times 30 \mu\text{m}$ in size. Positive secondary ions were extracted with a 10 kV

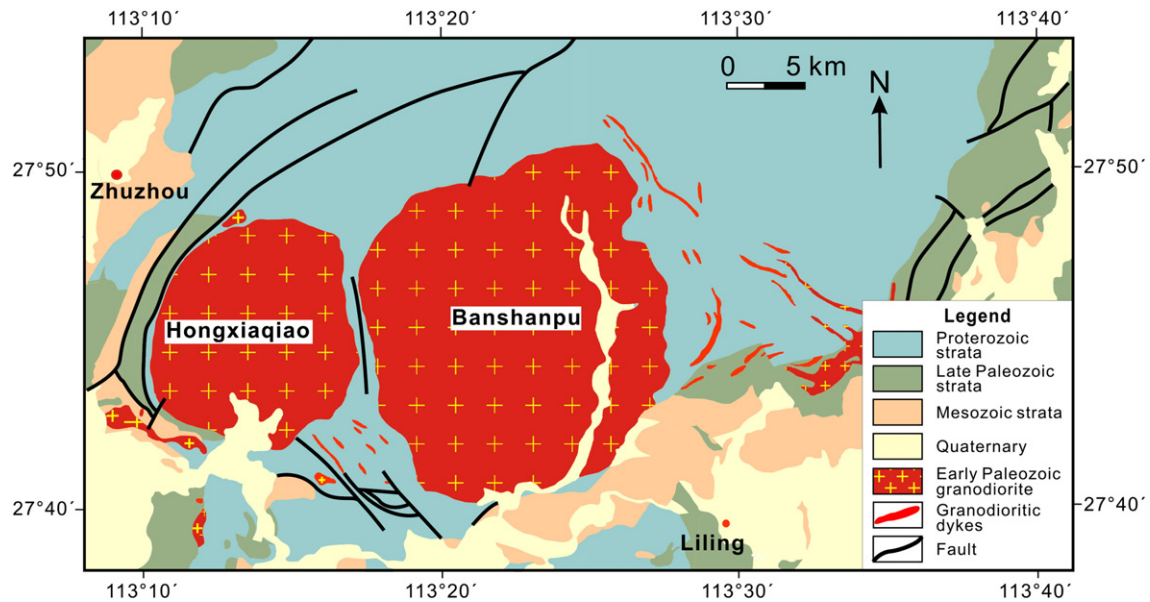


Fig. 2. Geological sketch map of the Banshanpu and Hongxiaqiao plutons.

potential. In the secondary ion beam optics, a 60 eV energy window was used, together with a mass resolution of ca. 5400 (at 10% peak height), to separate Pb^+ peaks from isobaric interferences. A single electron multiplier was used in ion-counting mode to measure secondary ion beam intensities by peak jumping mode. Analyses of the standard zircon Plešovice were interspersed with unknown grains. Each measurement consists of 7 cycles. Pb/U calibration was performed relative to zircon standard Plešovice (Sláma et al., 2008), while U and Th concentrations were calibrated against 91500 (Wiedenbeck et al., 1995). A long-term uncertainty of 1.5% (1σ RSD) for $^{206}Pb/^{238}U$ measurements of the standard zircons was propagated to the unknowns (Q.L. Li et al., 2010), despite that the measured $^{206}Pb/^{238}U$ error in a specific session is generally $\leq 1\%$ (1σ RSD). Measured compositions were corrected for common Pb using non-radiogenic ^{204}Pb . Corrections are sufficiently small to be insensitive to the choice of common Pb composition, and an average of present-day crustal composition (Stacey and Kramers, 1975) is used for the common Pb assuming that the common Pb is largely surface contamination introduced during sample preparation. Data reduction was carried out using the ISOPLOT 3.0 program (Ludwig, 2003). Uncertainties on individual analyses in data tables are reported at 1σ level; Concordia U–Pb ages are quoted with 95% confidence

interval, except where noted otherwise. In order to monitor the external uncertainties of SIMS U–Pb zircon dating calibrated against Plešovice standard, an in-house zircon standard Qinghu was alternately analyzed as an unknown together with other unknown zircons. Twenty-two measurements on Qinghu zircon yield a Concordia age of 160 ± 1 Ma, which is identical within error with the recommended value of 159.5 ± 0.2 Ma (Li et al., 2013b). The Cameca SIMS zircon U–Pb dating results are presented as supplementary online material in Appendix B.

3.2. Whole rock geochemical analyses

Rock samples were crushed into small chips and ultrasonically cleaned in distilled water with 5% HNO_3 and distilled water, then dried and handpicked to remove visible contamination. The rock chips were then ground in an agate mill, and the resulting powder was used for analyses of major and trace elements, and Sr–Nd isotopes, at GIGCAS. Major element oxides (wt.%) were determined on fused glasses with a 1:8 ratio of sample to $Li_2B_4O_7$ flux, using a Rigaku ZSX100e X-ray fluorescence spectrometer in the State Key Laboratory of Isotope Geochronology, GIGCAS. The accuracy of the XRF analyses is estimated at ca. 1% for SiO_2 , ca. 5% for MnO and P_2O_5 and ca. 2% for other major oxides (Li et al., 2003). Trace elements, including rare earth elements (REE), were analyzed on a Perkin-Elmer Sciex ELAN 6000 ICP-MS at GIGCAS, following procedures described by Li et al. (2002). Powdered samples (50 mg) were digested with mixed $HNO_3 + HF$ acid in steel-bomb coated Teflon beakers for two days in order to ensure complete dissolution of refractory minerals. An internal standard Rh solution was used to monitor signal drift. USGS rock standards G-2, W-2, MRG-1 and AGV-1 and the Chinese national rock standards GSD-12, GSR-1, GSR-2 and GSR-3 were used to calibrate elemental concentrations of the measured samples. Analytical precision was generally better than 5% (Li et al., 2002).

3.3. Sr–Nd isotopic analyses

After separation of Sr and Nd using a two-step exchange procedure, $^{87}Sr/^{86}Sr$ and $^{143}Nd/^{144}Nd$ ratios were measured with a Micromass IsoProbe multi-collector mass spectrometer (MC-ICP-MS) at the State Key Laboratory of Isotope Geochronology and Geochemistry, GIGCAS, following the procedures described by Wei et al. (2002) and Li et al.



Fig. 3. Outcrop picture of mafic microgranular enclaves (MME) in the Hongxiaqiao pluton.

(2004). Measured $^{87}\text{Sr}/^{86}\text{Sr}$ and $^{143}\text{Nd}/^{144}\text{Nd}$ ratios were normalized to $^{86}\text{Sr}/^{88}\text{Sr} = 0.1194$ and $^{146}\text{Nd}/^{144}\text{Nd} = 0.7219$, whereas the reported $^{87}\text{Sr}/^{86}\text{Sr}$ and $^{143}\text{Nd}/^{144}\text{Nd}$ ratios were adjusted to the NBS SRM 987 standard $^{87}\text{Sr}/^{86}\text{Sr} = 0.71025$ and the Shin Etsu JNdi-1 standard $^{143}\text{Nd}/^{144}\text{Nd} = 0.512115$, respectively.

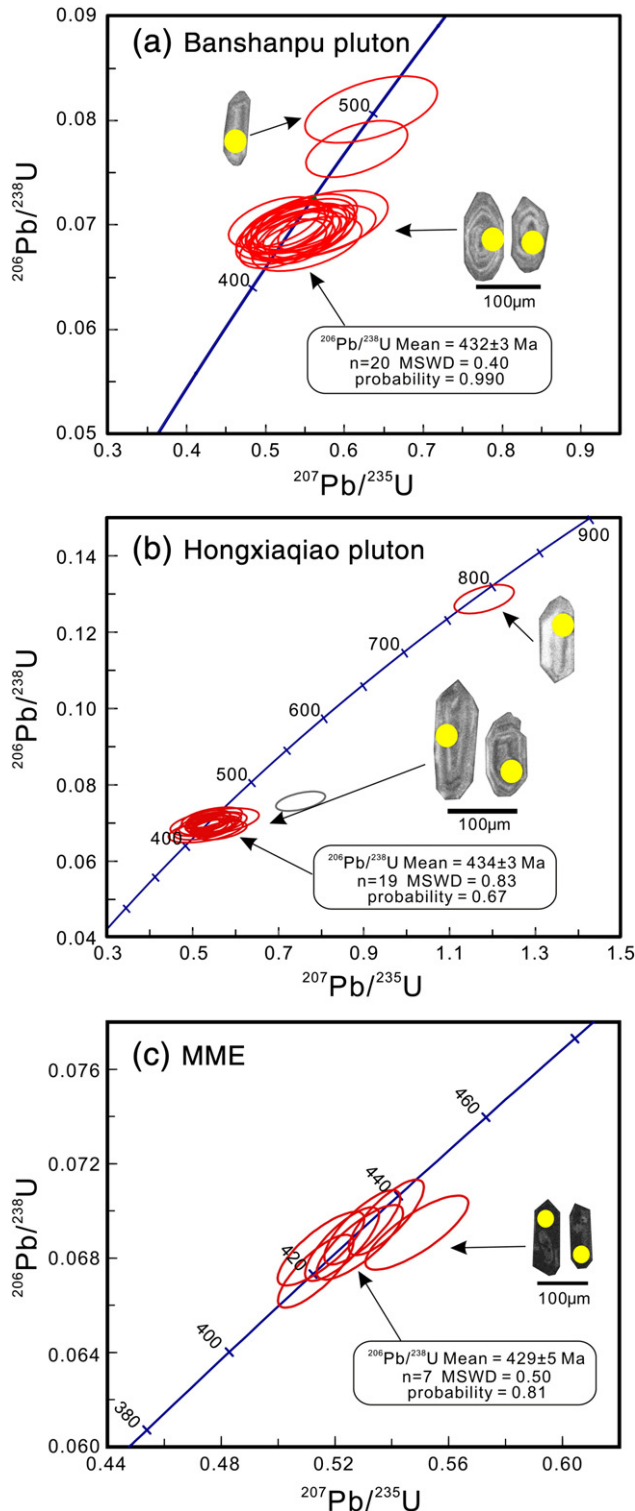


Fig. 4. Zircon U–Pb concordia diagrams and CL images of representative zircon grains (a) Banshanpu pluton; (b) Hongxiaqiao pluton; (c) MME within the Hongxiaqiao pluton.

4. Analytical results

4.1. Zircon U–Pb geochronology

4.1.1. The Banshanpu pluton

Sample YLL-1 from this pluton was processed for zircon separation. Zircon grains from the Banshanpu pluton are commonly transparent, stubby and prismatic without inherited cores (Fig. 4a). The zircon grains range in size from 60 to 150 μm , with length-to-width ratios between 1.5 and 2.0. Twenty two zircons were analyzed, and the analytical results are listed in Supplementary online material (Appendix A). Most grains have high Th/U ratios (0.59–1.19) and show concentric oscillatory zoning, indicating an igneous origin. Twenty spots yield $^{206}\text{Pb}/^{238}\text{U}$ ages between 425 Ma and 438 Ma (Supplementary online material), which form a coherent group with a weighted mean age of 432 ± 3 Ma (MSWD = 0.40) (Fig. 4a), indicating that the Banshanpu pluton was emplaced in the early Silurian. The other two analyses (YLL-1-19 and YLL-1-21) give concordant ages of 480 Ma and 502 Ma that are interpreted to be xenocryst incorporated from the wall-rocks.

4.1.2. The Hongxiaqiao pluton

Zircon grains for isotope analyses were separated from sample YH-1 of the Hongxiaqiao pluton. Zircon grains from the pluton are relatively large (80–200 μm) and elongated with length to width ratios ranging from 1.5 to 3.0 (Fig. 4b). Most grains are euhedral to subhedral, transparent and prismatic and display oscillatory zoning. Inherited cores are observed in some zircons. Twenty-one zircons were analyzed (Appendix A), and these have high Th/U ratios (0.42–3.27), consistent with an igneous origin. Nineteen analyses yield $^{206}\text{Pb}/^{238}\text{U}$ ages ranging from 424 Ma to 444 Ma, which record a weighted mean age of 434 ± 3 Ma (MSWD = 0.83) (Fig. 4b). This age is considered to reflect the emplacement time of the pluton. In addition, spot YH-1-9 gives an older $^{206}\text{Pb}/^{238}\text{U}$ age of 780 Ma which is interpreted to be xenocryst incorporated from the wall-rocks (Appendix A). Spot YH-1-13 gives a discordant age (apparent $^{206}\text{Pb}/^{238}\text{U}$ age = 470 ± 6 Ma).

4.1.3. MME within the Hongxiaqiao pluton

A MME sample (10BG2-4) was processed for zircon separation. Zircons are euhedral to subhedral, light-yellow to transparent crystals, generally less than 100 μm in size. Different from zircons of the host rocks, which occur as elongated crystals with concentric and oscillatory zoning, zircons from the MME samples are generally stubby crystals (length/width = 1–2.5) and display oscillatory zoning in CL images (Fig. 4c). No inherited cores were found. A total of 7 zircons were analyzed and all possess high Th/U ratios (0.362–1.797, Appendix B), which, together with their morphology and internal structure, indicate an igneous origin. Seven analyses of zircons from sample 10BG2-4 form a coherent group on the concordia diagram with a weighted mean $^{206}\text{Pb}/^{238}\text{U}$ age of 429 ± 5 Ma (Fig. 4c). The age is indistinguishable from the zircon U–Pb ages of their host within error (434 ± 3 Ma, Fig. 4b), confirming that the MMEs formed at the same time as their host.

4.2. Major oxides

Major oxide compositions of the samples are listed in Table 1. All the granitoid samples possess intermediate to high SiO_2 (64.0–69.7 wt.%) and Al_2O_3 (15.2–15.7 wt.%) contents. Samples from the Hongxiaqiao pluton fall in the granodiorite field in the TAS classification diagram, while those from the Banshanpu pluton exhibit transitional characteristics between the granodiorite and granite fields (Fig. 5). With an increase in SiO_2 , the Banshanpu pluton samples exhibit decreasing trends in most major oxides, whereas rocks from the Hongxiaqiao pluton show a decrease in TiO_2 , Fe_2O_3 , MgO and P_2O_5 , together with insignificant trends in Al_2O_3 , CaO and Na_2O (Table 1; Fig. 6). In comparison,

Table 1

Major oxide and trace element concentrations of the granitoid plutons and associated MMEs in the eastern Yangtze Block.

Sample	Banshanpu pluton												Hongxiaqiao pluton									
	YLL -1	YLL -2	YLL -3	YLL -4	YLL -5	YLL -6	YLL -7	YLL -8	YLL -9	YLL -10	YLL -11	YLL -12	YH -1	YH -2	YH -3	YH -4	YH -5	YH -6	YH -7	YH -8	YH -9	YH -10
<i>Major oxides (wt.%)</i>																						
SiO ₂	68.7	68.6	69.0	69.1	69.7	69.3	69.1	69.1	69.2	69.2	69.6	68.7	65.0	65.2	65.3	65.2	64.8	64.4	64.9	65.0	65.3	65.2
TiO ₂	0.41	0.42	0.41	0.40	0.40	0.38	0.42	0.41	0.42	0.40	0.37	0.43	0.58	0.61	0.60	0.58	0.62	0.60	0.60	0.60	0.61	0.59
Al ₂ O ₃	15.5	15.6	15.4	15.6	15.2	15.2	15.4	15.4	15.5	15.6	15.2	15.6	15.4	15.5	15.5	15.6	15.6	15.4	15.5	15.5	15.5	15.4
Fe ₂ O ₃ ^T	2.92	2.95	2.89	2.87	2.93	2.78	2.97	2.96	2.99	2.87	2.68	3.05	4.46	4.66	4.62	4.58	4.78	4.52	4.65	4.74	4.63	4.51
MnO	0.04	0.04	0.04	0.04	0.04	0.04	0.04	0.04	0.04	0.04	0.04	0.04	0.06	0.06	0.06	0.06	0.06	0.06	0.06	0.06	0.06	0.06
MgO	1.48	1.54	1.47	1.44	1.46	1.37	1.58	1.46	1.43	1.44	1.36	1.48	2.56	2.66	2.61	2.52	2.69	2.67	2.65	2.64	2.64	2.63
CaO	3.16	2.84	2.43	3.05	2.64	2.97	2.87	3.14	3.17	3.09	2.90	2.83	4.11	4.05	4.18	4.13	4.07	3.75	4.19	4.28	4.23	3.93
Na ₂ O	3.09	3.14	3.16	3.09	3.00	3.04	3.04	3.10	3.06	3.05	2.85	3.21	2.70	2.72	2.76	2.76	2.67	2.71	2.68	2.74	2.75	2.74
K ₂ O	3.10	3.14	3.17	2.89	3.12	3.24	2.97	2.71	2.87	3.17	3.46	2.78	3.17	3.26	3.10	3.14	3.12	3.20	3.21	3.16	3.18	3.32
P ₂ O ₅	0.10	0.10	0.10	0.10	0.11	0.08	0.11	0.11	0.11	0.10	0.09	0.12	0.16	0.17	0.17	0.16	0.16	0.16	0.16	0.16	0.16	0.17
LOI	1.33	1.51	1.84	1.35	1.29	1.38	1.36	1.47	1.06	0.90	1.32	1.68	1.72	0.93	0.98	1.07	1.22	2.52	1.28	0.95	0.84	1.33
Total	99.9	99.9	99.9	99.9	99.8	99.8	99.9	99.9	99.8	99.8	99.8	99.9	99.9	99.9	99.9	99.9	99.9	99.9	99.9	99.9	99.9	99.9
<i>Trace elements (ppm)</i>																						
Sc	6.43	6.38	6.84	6.70	6.67	6.78	7.17	6.08	6.91	6.46	7.85	5.57	12.8	12.3	12.5	11.7	14.0	13.9	12.7	12.1	13.0	13.0
V	49.3	47.8	49.3	52.5	48.6	50.6	51.1	51.2	53.2	54.5	45.4	51.7	87.0	87.5	83.6	93.3	100	92.2	93.1	97.1	92.7	88.6
Cr	29.9	25.9	25.9	40.4	24.9	28.3	26.2	28.4	27.3	28.5	27.2	25.7	69.6	63.2	67.9	193	75.9	73.6	75.3	200	78.0	73.0
Co	49.2	38.7	30.6	48.5	39.5	41.9	49.9	30.5	32.4	41.5	34.6	31.2	44.4	45.9	43.5	14.0	62.8	60.5	50.2	14.5	40.2	56.1
Ni	19.7	19.0	19.3	19.7	17.5	18.3	18.8	18.7	18.8	18.8	17.7	19.3	36.5	40.0	36.5	38.2	39.0	39.0	37.9	39.0	39.0	37.1
Cu	10.8	10.6	12.1	10.2	9.6	11.1	14.7	11.0	14.4	13.6	9.7	9.4	23.5	29.2	29.3	23.3	26.2	40.9	22.2	28.0	27.1	25.5
Zn	40.0	40.4	44.8	41.6	37.7	37.5	40.4	40.8	43.2	39.3	37.4	42.0	50.2	53.3	49.8	49.7	53.9	53.8	55.6	50.8	53.2	49.9
Ga	16.4	16.1	16.7	16.9	15.8	15.9	16.6	16.5	17.6	16.9	15.4	17.7	18.0	17.4	17.1	17.3	18.5	18.4	18.1	17.6	18.1	17.6
Rb	120	132	149	119	119	136	121	131	129	125	119	141	151	155	149	146	167	163	166	162	167	164
Sr	416	462	280	376	341	350	467	335	378	394	403	335	350	344	345	352	375	382	344	343	343	340
Y	9.42	9.61	9.08	9.87	9.55	9.34	9.97	9.95	10.7	9.21	8.51	9.99	16.0	16.1	16.1	14.8	17.3	16.5	16.0	15.8	16.9	17.3
Zr	185	147	166	162	180	181	179	197	185	176	180	199	202	208	214	236	224	226	215	193	210	197
Nb	7.24	6.27	7.09	7.37	7.60	7.07	7.66	7.96	8.29	7.26	6.13	8.94	9.00	9.19	9.07	8.71	9.68	9.20	9.01	9.13	9.92	9.61
Cs	8.34	4.92	8.33	6.07	10.5	4.17	10.3	12.3	9.53	10.1	3.55	13.4	9.79	10.7	10.1	9.18	10.2	11.0	8.01	9.97	15.7	14.5
Ba	753	726	635	626	810	726	771	567	762	823	890	556	783	822	760	796	819	852	784	804	797	753
La	40.0	30.7	33.6	28.9	25.9	25.3	29.8	28.0	25.0	33.4	24.2	33.0	35.8	34.2	33.3	31.1	30.9	34.2	37.9	34.5	31.2	40.0
Ce	73.2	59.3	63.8	54.0	50.4	47.2	58.5	51.4	48.6	63.1	45.8	62.8	70.2	69.4	68.8	64.3	65.9	71.4	76.5	72.4	65.6	80.6
Pr	8.02	6.69	7.15	6.13	5.71	5.32	6.54	5.92	5.45	7.09	5.32	7.16	8.55	8.66	8.32	7.75	8.05	8.75	9.01	8.67	7.96	9.74
Nd	25.1	21.0	21.8	19.6	18.8	17.3	21.7	18.9	18.5	22.2	17.5	23.2	29.5	29.3	29.2	26.7	28.8	30.2	30.7	30.0	27.5	32.6
Sm	3.48	3.10	3.15	2.95	2.88	2.73	3.32	2.98	3.06	3.23	2.85	3.27	4.74	4.63	4.75	4.34	4.94	4.89	4.79	4.85	4.62	5.08
Eu	0.75	0.70	0.71	0.74	0.67	0.69	0.77	0.74	0.77	0.71	0.77	0.75	0.99	0.97	1.00	0.93	1.04	0.98	1.00	1.02	0.95	0.96
Gd	2.64	2.38	2.29	2.36	2.21	2.29	2.59	2.44	2.57	2.28	2.32	2.45	3.90	3.44	3.68	3.53	3.95	3.73	3.76	3.72	3.69	3.91
Tb	0.31	0.32	0.31	0.32	0.31	0.30	0.31	0.32	0.36	0.29	0.29	0.33	0.51	0.46	0.51	0.47	0.52	0.52	0.49	0.48	0.52	0.54
Dy	1.72	1.67	1.58	1.74	1.61	1.66	1.78	1.74	1.89	1.55	1.57	1.79	2.73	2.62	2.78	2.64	2.93	2.87	2.76	2.71	2.83	3.03
Ho	0.31	0.29	0.28	0.31	0.31	0.30	0.32	0.32	0.34	0.29	0.28	0.33	0.52	0.50	0.52	0.50	0.56	0.54	0.53	0.51	0.55	0.59
Er	0.82	0.81	0.75	0.82	0.83	0.81	0.84	0.82	0.92	0.71	0.70	0.89	1.40	1.32	1.37	1.35	1.49	1.47	1.47	1.38	1.45	1.56
Tm	0.12	0.11	0.11	0.12	0.12	0.12	0.13	0.13	0.14	0.11	0.10	0.13	0.22	0.20	0.21	0.21	0.23	0.23	0.22	0.21	0.22	0.24
Yb	0.80	0.76	0.73	0.78	0.84	0.78	0.86	0.84	0.91	0.74	0.67	0.82	1.45	1.35	1.37	1.39	1.54	1.55	1.49	1.42	1.52	1.55
Lu	0.13	0.11	0.12	0.12	0.13	0.12	0.13	0.13	0.13	0.12	0.10	0.13	0.23	0.22	0.22	0.22	0.25	0.25	0.23	0.23	0.24	0.24
Hf	4.85	3.73	4.32	4.01	4.77	4.48	4.90	4.90	4.78	4.43	4.43	4.86	5.51	5.37	5.53	6.31	5.77	6.22	5.87	5.13	5.73	5.35
Ta	0.84	0.58	0.76	0.88	0.84	0.81	0.94	0.88	0.92	0.77	0.58	0.85	0.96	0.94	0.92	0.82	1.09	1.05	0.96	0.87	1.22	1.03
Pb	113	105	97.8	109	109	102	116	98.9	119	120	108	115	126	121	123	120	131	138	125	128	133	131
Th	20.4	17.9	19.3	19.3	15.2	14.6	18.1	15.9	18.2	20.2	13.7	19.9	23.1	21.4	23.0	21.7	25.4	26.7	24.6	24.7	22.2	26.8
U	2.77	3.05	3.25	3.06	4.37	3.24	3.88	3.77	3.33	3.50	2.13	4.98	3.54	3.21	3.55	4.10	4.29	5.28	5.23	4.90	4.11	7.05
La _N /Yb _N	35.8	29.1	33.2	26.6	22.2	23.2	24.8	23.8	19.6	32.4	25.9	29.0	17.7	18.2	17.4	16.0	14.4	15.8	18.3	17.4	14.7	18.5
Eu/Eu*	0.76	0.78	0.80	0.85	0.81	0.85	0.80	0.84	0.84	0.80	0.92	0.81	0.71	0.75	0.73	0.72	0.72	0.70	0.72	0.74	0.70	0.66
Mg#	54.1	54.9	54.4	54.0	53.8	53.4	55.3	53.5	52.7	53.9	54.1	53.0	57.2	57.0	56.8	56.2	56.8	58.0	57.0	56.5	57.0	57.6

Mg# = 100*Mg/(Mg + Fe²⁺), assuming Fe²⁺/Fe^{total} = 0.85; LOI = loss of ignition; Fe₂O₃^T = total Fe oxides as Fe₂O₃; footnote N means chondrite normalization.

Table 1 (continued)

Sample	Hongxiaqiao pluton																		MME								
	YH	YH	YH	YH	YH	YH	YH	YH	YH	YH	YH	YH	YH	YH	YH	YH	YH	YH	10BG	10BG	10BG	10BG	10BG	10BG	10BG		
	–11	–12	–13	–14	–15	–16	–17	–18	–19	–20	–21	–22	–23	–24	–25	–26	–27	–28	1-01	1-02	1-04	1-06	2-3	2-4	2-5		
<i>Major oxides (wt.%)</i>																											
SiO ₂	65.2	64.0	64.2	64.9	65.3	65.0	64.8	64.4	64.5	65.0	64.6	65.2	65.0	65.2	65.3	65.4	64.9	64.2	55.9	53.2	53.2	54.9	58.7	53.2	52.2		
TiO ₂	0.59	0.60	0.63	0.59	0.58	0.59	0.57	0.61	0.63	0.59	0.61	0.60	0.59	0.61	0.58	0.58	0.61	0.64	0.86	0.81	0.80	0.92	0.85	0.84	0.85		
Al ₂ O ₃	15.4	15.4	15.6	15.5	15.5	15.5	15.4	15.6	15.6	15.6	15.5	15.6	15.7	15.6	15.7	15.5	15.5	15.6	17.0	16.7	16.7	17.1	17.8	13.8	13.8		
Fe ₂ O ₃	4.51	4.66	4.76	4.48	4.38	4.52	4.43	4.68	4.79	4.51	4.57	4.56	4.60	4.71	4.49	4.48	4.63	5.08	7.39	8.35	8.34	7.89	6.17	7.33	7.3		
MnO	0.06	0.07	0.07	0.06	0.06	0.06	0.06	0.06	0.07	0.06	0.07	0.06	0.07	0.07	0.06	0.06	0.06	0.07	0.15	0.17	0.17	0.15	0.09	0.11	0.11		
MgO	2.60	2.76	2.82	2.57	2.50	2.57	2.55	3.06	2.77	2.63	2.67	2.67	2.59	2.73	2.62	2.55	2.69	2.88	4.93	5.84	5.90	5.25	2.98	9.28	8.56		
CaO	4.18	4.12	3.73	3.93	3.89	3.92	3.81	3.49	4.34	4.15	4.15	3.34	3.97	4.39	4.36	4.24	4.01	4.42	6.02	6.91	6.89	6.15	5.08	5.96	6.19		
Na ₂ O	2.67	2.59	2.63	2.65	2.66	2.65	2.64	2.80	2.60	2.61	2.75	2.70	2.71	2.73	2.75	2.63	2.50	2.65	2.88	3.06	2.97	2.91	3.13	1.97	2.29		
K ₂ O	3.33	3.35	3.28	3.32	3.34	3.36	3.30	3.29	3.14	3.20	3.23	3.15	3.31	2.95	3.07	3.27	3.41	3.07	2.72	2.10	2.22	2.61	2.79	3.21	1.50		
P ₂ O ₅	0.17	0.17	0.17	0.16	0.15	0.16	0.16	0.18	0.17	0.16	0.17	0.16	0.16	0.17	0.16	0.17	0.16	0.17	0.23	0.40	0.37	0.26	0.24	0.28	0.28		
LOI	1.24	2.18	2.00	1.69	1.53	1.50	2.21	1.73	1.30	1.44	1.61	1.82	1.16	0.74	0.83	0.96	1.49	1.15	1.41	2.04	1.95	1.45	1.76	3.68	6.89		
Total	99.9	99.9	99.9	99.9	99.9	99.9	99.9	99.9	99.9	99.9	99.9	99.9	99.9	99.9	99.9	99.9	99.9	99.9	99.6	99.6	99.6	99.6	99.6	99.6	100.0		
<i>Trace elements (ppm)</i>																											
Sc	12.8	14.0	13.4	12.4	11.4	11.3	12.4	14.1	13.2	13.2	13.6	12.2	12.3	13.4	12.4	11.4	12.9	13.5	17.6	18.9	18.4	18.5	11.8	16.1	16.0		
V	90.6	111	94.5	84.6	80.8	81.4	85.7	93.7	94.7	89.3	101	82.9	93.9	91.7	85.7	82.0	87.0	115	110	112	113	120	100	100	101		
Cr	65.7	85.2	72.0	66.0	58.9	61.9	65.2	77.9	78.0	61.7	73.9	60.6	209	79.4	66.6	58.7	63.5	202	132	154	155	119	69.5	418	424		
Co	42.0	52.1	40.3	41.4	45.7	37.6	33.6	45.6	47.7	49.3	58.6	38.4	14.2	41.2	47.9	44.4	44.3	16.1	16.7	20.7	21.2	18.0	12.7	25.7	24.3		
Ni	35.7	40.8	36.6	35.5	33.7	34.1	38.0	40.1	38.2	35.4	38.5	34.8	38.1	38.6	38.5	34.3	37.8	40.8	30.5	71.8	73.7	30.0	11.9	171	145		
Cu	19.5	29.6	26.7	74.2	71.4	75.2	70.2	17.9	44.3	21.8	22.2	59.8	22.5	30.9	20.6	29.0	49.5	34.7	141	178	167	150	47.6	7.9	9.4		
Zn	51.5	57.8	53.8	50.9	48.2	48.4	51.2	50.9	54.1	47.7	52.3	49.2	53.9	53.0	50.5	46.5	52.6	54.0	60.1	65.5	65.6	64.2	44.1	52.6	60.0		
Ga	16.8	18.1	18.2	17.9	17.2	16.8	17.6	17.6	18.1	17.3	17.7	17.0	18.1	18.5	18.1	16.3	18.8	17.4	14.0	14.7	14.5	14.2	13.6	11.2	11.5		
Rb	144	157	163	161	153	174	155	157	168	150	180	157	167	171	154	144	178	146	111	87.7	96.7	118	101	165	66.2		
Sr	327	343	349	349	337	342	320	410	361	371	364	352	376	355	364	334	363	353	193	218	224	188	240	171	157		
Y	15.7	17.1	17.2	16.2	15.7	15.8	15.5	17.2	16.4	15.6	16.6	15.2	15.5	17.8	15.9	14.6	16.5	16.9	18.6	25.5	25.7	19.9	13.9	10.9	11.1		
Zr	198	194	219	205	220	188	201	213	208	199	199	198	211	210	201	192	239	192	152	293	284	152	162	151	151		
Nb	8.76	9.33	9.28	8.70	9.20	9.18	9.19	8.81	9.43	8.56	9.13	8.88	8.64	10.4	8.75	8.30	8.99	9.09	10.6	11.8	11.6	11.9	7.47	6.53	6.75		
Cs	10.5	11.5	15.0	10.6	10.4	12.0	9.34	10.7	12.1	10.9	14.1	13.1	16.9	16.9	14.8	8.18	11.0	9.63	9.94	3.93	5.71	11.5	7.50	25.5	12.2		
Ba	783	797	851	792	745	783	785	870	769	803	845	849	839	761	744	798	849	804	477	479	432	472	524	430	226		
La	35.6	37.0	41.4	35.6	34.2	37.6	40.9	36.5	41.0	35.6	37.4	39.7	32.8	38.7	32.4	35.3	36.0	23.1	10.0	27.7	25.1	10.2	32.2	24.7	24.3		
Ce	73.0	76.3	84.4	73.1	68.8	75.2	82.9	73.5	82.8	72.8	75.4	77.8	68.5	79.4	66.7	70.5	73.9	52.2	30.3	69.4	64.4	31.8	64.2	55.1	55.0		
Pr	8.84	9.53	10.2	8.97	8.22	8.88	9.91	8.94	9.88	9.02	9.12	9.18	8.50	9.70	8.03	8.54	8.60	7.05	5.13	10.3	10.1	5.42	7.82	7.36	7.38		
Nd	29.8	32.6	33.7	30.8	27.6	29.7	32.8	30.4	32.5	30.1	31.0	30.4	29.1	33.0	28.0	28.6	29.7	26.2	23.8	44.2	43.5	25.6	28.3	29.7	29.7		
Sm	4.73	5.34	5.12	4.74	4.50	4.58	4.83	4.87	5.01	4.73	4.99	4.71	4.66	5.23	4.47	4.42	4.83	4.61	5.27	8.52	8.39	5.59	4.48	4.54	4.56		
Eu	0.97	1.05	1.03	0.99	0.97	0.97	0.95	1.02	1.04	0.97	1.01	1.00	0.97	1.03	0.95	0.91	1.00	1.00	1.07	1.47	1.47	1.09	0.98	0.94	1.00		
Gd	3.70	4.09	3.89	3.58	3.57	3.34	3.68	3.87	3.97	3.51	3.85	3.61	3.51	4.12	3.60	3.35	3.73	3.56	4.26	6.65	6.65	4.45	3.73	3.25	3.40		
Tb	0.51	0.55	0.53	0.49	0.46	0.48	0.47	0.52	0.53	0.48	0.53	0.46	0.48	0.55	0.50	0.44	0.50	0.51	0.68	0.97	0.97	0.72	0.51	0.45	0.46		
Dy	2.80	3.03	2.90	2.70	2.57	2.66	2.66	2.86	2.85	2.66	2.90	2.60	2.65	3.02	2.68	2.42	2.78	2.79	3.81	5.20	5.15	4.02	2.76	2.23	2.30		
Ho	0.54	0.58	0.56	0.52	0.50	0.52	0.52	0.55	0.55	0.51	0.55	0.49	0.52	0.58	0.51	0.47	0.52	0.55	0.77	1.03	1.01	0.83	0.55	0.45	0.45		
Er	1.43	1.51	1.47	1.39	1.33	1.37	1.37	1.46	1.48	1.37	1.45	1.30	1.38	1.53	1.36	1.24	1.42	1.45	2.10	2.88	2.81	2.21	1.58	1.21	1.26		
Tm	0.22	0.22	0.22	0.21	0.21	0.21	0.22	0.22	0.22	0.20	0.22	0.20	0.22	0.23	0.21	0.19	0.22	0.22	0.31	0.40	0.40	0.32	0.22	0.18	0.18		
Yb	1.47	1.53	1.54	1.43	1.38	1.39	1.44	1.49	1.51	1.39	1.49	1.30	1.41	1.56	1.40	1.28	1.46	1.48	2.00	2.63	2.62	2.11	1.55	1.15	1.21		
Lu	0.23	0.24	0.24	0.23	0.22	0.22	0.22	0.23	0.24	0.22	0.23	0.21	0.22	0.25	0.22	0.19	0.23	0.23	0.30	0.39	0.39	0.31	0.23	0.18	0.18		
Hf	5.43	5.34	5.91	5.65	5.96	5.03	5.45	5.69	5.67	5.44	5.36	5.03	5.57	5.76	5.20	5.09	6.37	5.21	4.95	9.29	9.23	4.96	5.12	4.83	4.84		
Ta	0.91	0.98	0.95	1.02	0.99	1.07	1.02	0.97	0.98	0.94	1.04	0.87	0.85	1.16	0.93	0.82	0.96	0.85	1.09	1.11	1.07	1.24	0.73	0.53	0.55		
Pb	133	118	112	157	137	164	177	122	120	114	129	108	131	141	128	124	121	121	30.4	27.7	27.0	29.9	28.2	26.1	39.2		
Th	26.5	23.2	25.6	25.5	23.6	24.4	25.9	27.6	25.7	22.8	26.3	23.9	24.6	27.4	21.9	22.8	25.6	19.6	12.8	22.2	27.0	16.4	24.1	29.7	29.5		
U	4.89	5.37	5.01	4.76	5.36	4.99	4.64	5.62	4.44	4.92	5.69	5.00	5.41	6.92	4.75	4.45	4.65	4.39	3.87	6.21	6.66	4.15	3.82	4.24	4.35		
La _N /Yb _N	17.4	17.4	19.3	17.9	17.9	19.4	20.3	17.5	19.5	18.4	17.9	21.9	16.7	17.8	16.7	19.8	17.7	11.2	3.59	7.55	6.88	3.47	14.9	15.4	14.4		
Eu/Eu*	0.71	0.69	0.70	0.73	0.74	0.75	0.69	0.72	0.71	0.73	0.71	0.74	0.74	0.68	0.72	0.72	0.72	0.76	0.69	0.60	0.60	0.67	0.73	0.75	0.78		
Mg#	57.4	58.0	58.0	57.2	57.0	57.0	57.2	60.4	57.4	57.6	57.7	57.8	56.7	57.4	57.6	57.0	57.5	56.9	60.9	62.0	62.2	60.8	53.0	74.7	73.2		

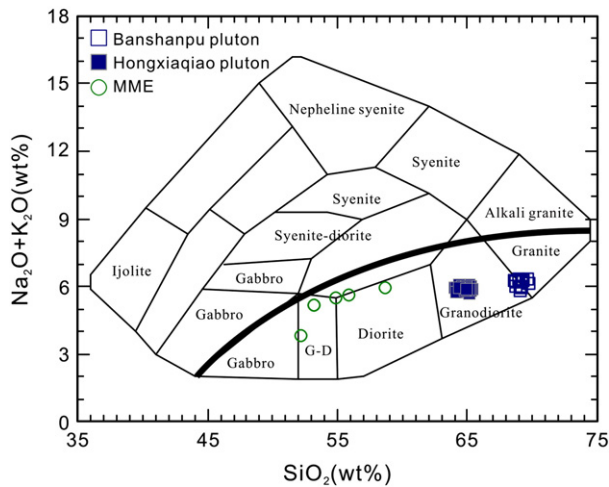


Fig. 5. Nomenclature diagram for the granitoid and MME rocks from the eastern Yangtze Block (after Cox et al., 1979; Wilson, 1989) (Solid line represents the boundary between alkaline and sub-alkaline rocks).

the Banshanpu pluton rocks are strongly peraluminous ($A/CNK > 1.1$) and have intermediate- to high-K calc-alkaline compositions, whereas samples from the Hongxiaqiao pluton seem to be more K-enriched ($K_2O/Na_2O = 1.08\text{--}1.36$) and mostly exhibit weak peraluminous characteristics (Fig. 7a, b).

MME samples from the Hongxiaqiao pluton possess wide ranges of SiO_2 (52–59 wt.%) and Al_2O_3 (13.8–17.8 wt.%) (Table 1), and their variably high K_2O contents (1.50–3.21 wt.%) indicate calc-alkaline to high-K calc-alkaline characteristics (Fig. 7b). In spite of their wide range of MgO (2.98–9.28 wt%), the MME samples all show relatively high Mg# (53–75), and their P_2O_5 contents (0.23–0.40 wt.%) are significantly higher than those of coeval high-Mg basalt and gabbro (<0.24 wt.%) in the Cathysia Block (Y.J. Wang et al., 2013; Yao et al., 2012). In the TAS classification diagram, most MME samples fall in the diorite fields (Fig. 5).

4.3. Trace and rare earth elements

All the granodiorite and MME samples exhibit LREE-enriched patterns (Fig. 8), and there is no significant trend of total REE with increasing SiO_2 (not shown). Samples from the Banshanpu pluton have relatively low HREE ($Yb = 0.67\text{--}0.91$ ppm) and are characterized by strongly fractionated patterns ($(La/Yb)_N = 20\text{--}36$; $(Gd/Yb)_N = 2.2\text{--}2.9$), with weak negative Eu-anomalies ($Eu/Eu^* = 0.76\text{--}0.92$). Samples from the Hongxiaqiao pluton are more REE-enriched ($\Sigma REE = 125\text{--}187$ ppm) and exhibit intermediate REE fractionation ($(La/Yb)_N = 11\text{--}22$; $(Gd/Yb)_N = 2.0\text{--}2.3$). The MME samples have variable REE contents (90–182 ppm), but all exhibit mild REE fractionation ($(La/Yb)_N = 3\text{--}15$; $(Gd/Yb)_N = 1.7\text{--}2.3$) although their negative Eu anomalies ($Eu/Eu^* = 0.60\text{--}0.78$) are equivalent to, or slightly stronger, than those of their host rocks ($Eu/Eu^* = 0.66\text{--}0.76$) (Fig. 8c).

Samples from the Banshanpu and Hongxiaqiao plutons share some similarities in their trace element characteristics, and they all possess relatively high contents of large ion lithophile elements (LILE) (Fig. 8d, e), e.g. Rb (119–180 ppm), Sr (280–467 ppm), Ba (556–890 ppm), U (2.13–7.05 ppm) and Th (13.7–27.6 ppm). Comparatively, the Banshanpu pluton samples have lower levels of high field strength elements (HFSE), e.g. Zr, Nb, Hf, Ta and Y, and consequently higher Sr/Y ratios (31–48) than those of the Hongxiaqiao pluton samples, while samples from the Hongxiaqiao pluton possess higher levels of transitional metals (e.g. V, Cr, Ni, Sc and Zn), consistent with their relatively high TiO_2 , Fe_2O_3 and MgO contents. The Hongxiaqiao pluton samples also contain higher HFSE than those of the Banshanpu pluton samples. For example, the Hongxiaqiao pluton samples have Y contents (14.6–17.8 ppm) almost

twice as high as those of the Banshanpu pluton samples (8.51–10.7 ppm), which make their Sr/Y ratios (20–24) significantly lower. In the Sr/Y versus Y diagram (Fig. 9), samples from Banshanpu pluton fall in the adakite field, whereas samples from Hongxiaqiao pluton simply display transitional characteristics between adakite and normal arc rocks (Fig. 9). Samples from the Banshanpu and Hongxiaqiao plutons possess almost identical Nb/Ta (8.1–10.9) and Zr/Hf (36.2–41) ratios, which are distinct from those of the MME samples (Nb/Ta = 9.6–12.4; Zr/Hf = 30.6–31.7).

The MME samples have transitional metal element and LILE higher and lower than those of the granodiorite samples, respectively (Table 1). Their variable HFSE concentrations span the ranges of samples of the Banshanpu and Hongxiaqiao plutons. All the MME samples possess low Sr/Y ratios (9–17), which are quite close to those of coeval gabbro and high-Mg basalt in South China (Y.J. Wang et al., 2013; Yao et al., 2012).

4.4. Sr–Nd isotopic compositions

Sr–Nd isotope compositions of the rock samples are listed in Table 2. Although samples from the Banshanpu and Hongxiaqiao plutons show distinct characteristics in major and trace element compositions, Nd–Sr isotope compositions for the Banshanpu pluton ($\epsilon Nd_T = -7.47$ to -6.88 ; $^{87}Sr/^{86}Sr_i = 0.7121\text{--}0.7169$) and the Hongxiaqiao pluton ($\epsilon Nd_T = -8.32$ to -7.28 ; $^{87}Sr/^{86}Sr_i = 0.7109\text{--}0.7149$) samples mostly overlap and are almost indistinguishable from those of the MME samples ($\epsilon Nd_T = -7.45$ to -7.03 ; $^{87}Sr/^{86}Sr_i = 0.7115\text{--}0.7143$). In the Nd–Sr isotope correlation diagram, all the granitoid and MME samples fall in the field of Early Paleozoic granites of the eastern Yangtze Block (Fig. 10), implying a strong affinity to this crustal source. The samples display relatively small amounts of Sm/Nd fractionation ($f_{Sm/Nd} = -0.29$ to -0.54), and all exhibit Mesoproterozoic model ages irrespective of assumptions on their evolutionary history (single-stage or two-stage) (Table 2).

5. Discussion

5.1. Source and petrogenesis

5.1.1. The Banshanpu pluton

Rocks of the Banshanpu pluton are peraluminous ($A/CNK > 1.1$), and have low Y (<10.7 ppm), HREE ($Yb < 0.91$ ppm) but high Sr (280–462 ppm) contents, characterized by high Sr/Y (31–48) and $(La/Yb)_N$ (20–36) ratios. These characteristics are similar to those of adakite (Fig. 9) (Defant and Drummond, 1990), and imply a basaltic source in a pressure–temperature field where garnet \pm amphibole is stable but plagioclase is not (i.e., eclogite, garnet amphibolite or amphibolite) (Garrison and Davidson, 2003).

Adakites were originally defined as sodic, intermediate to silicic rocks, characterized by high SiO_2 (>56 wt%), Al_2O_3 (mostly > 15 wt%) and low MgO (usually < 3 wt%), with high Sr (>400 ppm), low Y (<18 ppm) and HREE ($Yb < 1.9$ ppm). The above characteristics, together with high Sr/Y ratios (mostly >40) and strikingly fractionated REE ($La/Yb > 20$) of adakites, imply a genesis by partial melting of subducted slab in the garnet stability field (Defant and Drummond, 1990). More recently, a large group of rocks with trace element characteristics similar to those of adakite has been reported in collision-related environment (e.g. Chung et al., 2003; Wang et al., 2005; Xu et al., 2002). In comparison with typical adakites, rocks of this group are relatively K-rich and has been classified as “K-adakites”, “continental adakites” or “C-type adakites” (Moyen, 2009; Xiao and Clemens, 2007). In addition, Kolb et al. (2013) use “adakite-like” to describe calc-alkaline arc rocks that share similar trace-element signatures, but have distinct major element concentrations from those of typical adakites. It appears that adakites and adakite-like rocks cover a wide spectrum and their lithological complexity is closely related to their petrogenetic diversity (Moyen, 2009 and references therein).

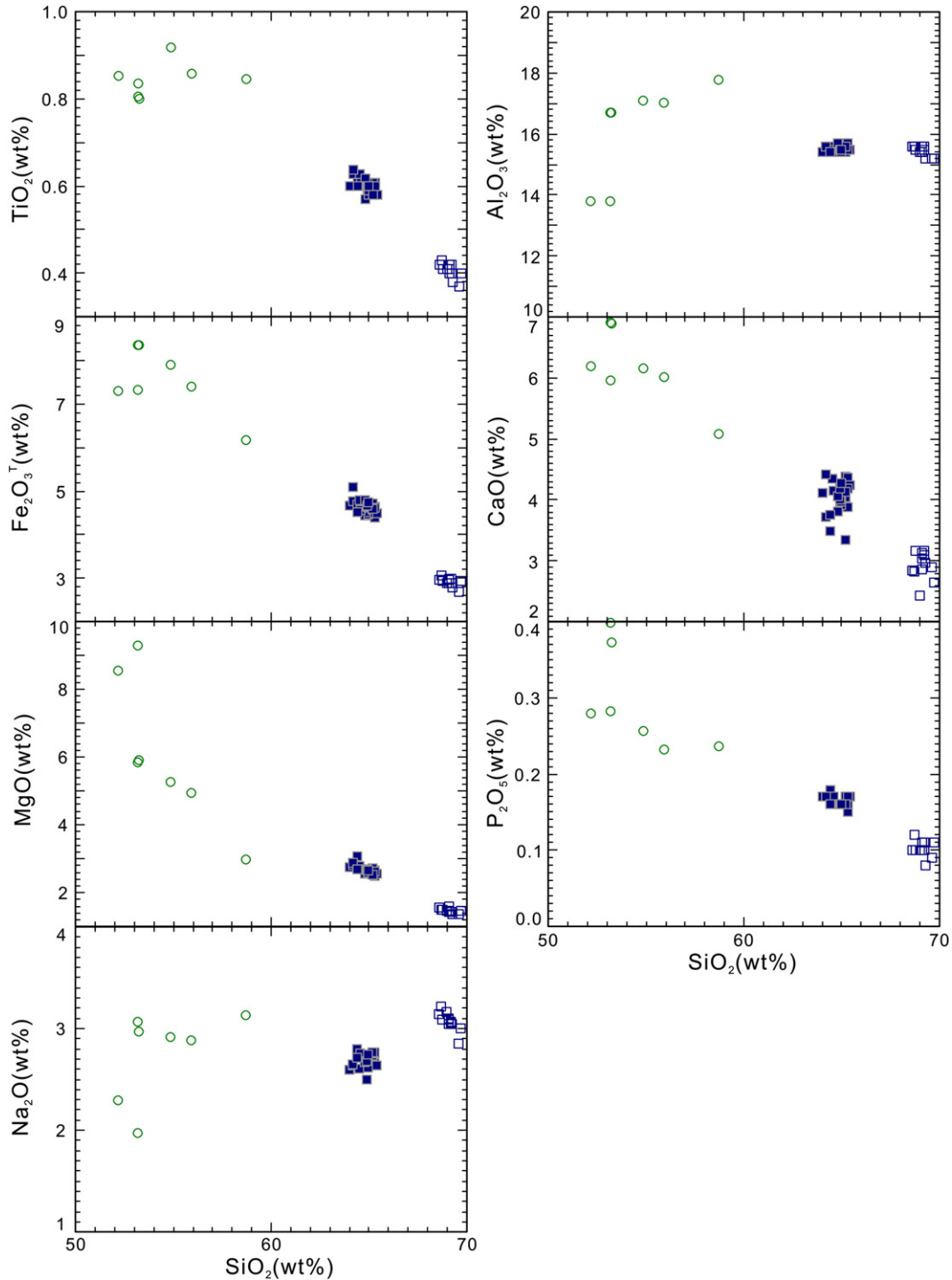


Fig. 6. Harker diagrams for the granitoid and MME samples (symbols are as in Fig. 5).

A distinct feature, namely adakitic signature, of adakites and adakites-like rocks is the low HREE and high Sr concentrations, which are generally interpreted in terms of amphibole, garnet, and plagioclase stability because of their high compatibility for these elements (Kay and Kay, 1991; Moyen, 2009). Both amphibole and garnet fractionation can lead to Y and HREE depletion, while the enrichment of Sr is generally ascribed to the retarded crystallization of plagioclase in water-rich magmas (Grove et al., 2002; Müntener et al., 2001). In addition to the slab-melting model, other models have also been proposed to account for the genesis of adakitic signature, including: (1) partial melting of previously existing TTG or adakitic rocks (Kamei et al., 2009; Watkins et al., 2007); (2) partial

melting of delaminated lower crust and interacting to some extent with mantle material (Kay and Kay, 1993; Xu et al., 2002); (3) mixing between crust- and mantle-derived magmas (Guo et al., 2007); (4) high pressure fractional crystallization of mantle-derived primitive arc magma (Castillo, 2006; Macpherson et al., 2006; Richards and Kerrich, 2007); and (5) partial melting of thickened lower crust (Atherton and Petford, 1993; Chung et al., 2003; Wang et al., 2005). Because rocks of the Banshanpu pluton have SiO_2 contents (<70 wt%) strikingly lower, and Cr (25–40 ppm) and Ni (17–20 ppm) contents significantly higher than those of “pseudo-adakite” ($\text{SiO}_2 > 73$ wt%; Cr ≤ 12 ppm; Ni ≤ 12 ppm) (Kamei et al., 2009), genesis of the Banshanpu pluton by partial melting

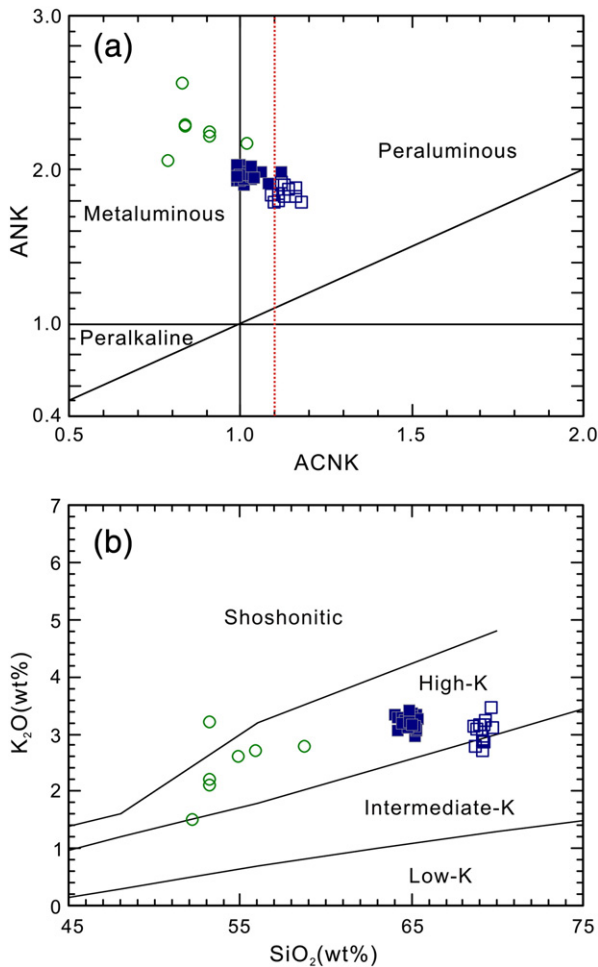


Fig. 7. (a) ANK-ACNK diagram (after Maniar and Piccoli, 1989); (b) K_2O vs. SiO_2 correlation diagram (after Le Maitre et al., 1989) for granitoids and MME from the eastern Yangtze Block. Symbols are as in Fig. 5.

of cryptic adakitic rocks seems unlikely. Likewise, partial melting of delaminated lower crust and magma mixing are unrealistic either because of the relatively low Mg# (~50) of the rocks and the lack of MME in the pluton. Other models mainly involve two processes, i.e. high-pressure fractionation of hydrous magmas and partial melting of lower crust in the garnet stability field. Fractionation of both garnet and amphibole can significantly decrease the HREE and Y levels in residual melt (Davidson et al., 2007; Macpherson et al., 2006). Apart from garnet and hornblende, some accessory minerals (e.g. titanite, apatite and zircon) possess high partitioning coefficients of REE and their fractional crystallization may decrease the REE levels in residual melt (Li et al., 2013a). Of the accessory minerals, some prefer to incorporate HREE (e.g. titanite and zircon) while others are strongly enriched in LREE (e.g. apatite) (Hoskin et al., 2000; Stefan and Stephan, 2006; Tiepolo et al., 2002), and removal of these accessory minerals will give rise to counterbalanced effect and produce limited influence on the REE patterns of the residual magma. Because high-pressure crystallization of garnet and hornblende consumes iron and magnesium and requires high H_2O contents (>3 wt%) (Alonso-Perez et al., 2009; Müntener et al., 2001), it is commonly invoked to account for the evolution of primary arc magmas in subduction zones (e.g. Coldwell et al., 2011; Davidson et al., 2007; Hidalgo et al., 2011; Rodríguez et al., 2007), where dehydration of subducting slab may generate high water flux to the mantle wedge and cause abundant arc magmas. In the case of granitoids, however, it has been demonstrated that it is difficult to generate peraluminous I-type granitic melt by removal of amphibole, and experimental work has demonstrated that

dehydration melting of basaltic to andesitic rocks is capable of generating peraluminous melt below garnet stability field where breakdown of biotite and amphibole will yield pyroxene and give rise to the excess Al and H_2O in the melt (Chappell et al., 2012 and reference therein). I-type granite by dehydration melting is commonly silica-oversaturated, normal to high-K calc-alkaline and markedly undersaturated in water, which, together with the relatively high viscosity, makes differentiation of granitic magma difficult (Clemens and Stevens, 2012 and references therein).

Like most I- and S-type granites, adakites and adakite-like rocks can be generated by dehydration or hydrous partial melting of mafic lower crust in both subduction-related environments and post-collisional settings (e.g. Atherton and Petford, 1993; Chung et al., 2003). Discerning between high-pressure fractionation and lower-crustal melting is difficult, and field evidence (e.g. lithological association and proportion of adakites or adakitic rocks) must be taken into account. There are numerous examples showing that adakites in subduction-related environment are commonly associated with abundant mafic and ultramafic rocks (e.g. Castillo, 2006; Dessimoz et al., 2012; Macpherson et al., 2006), which represent the parental magma evolving into adakites or adakite-like rocks through high-pressure fractionation. Because the Wuyi-Yunkai Orogen is an intra-continental orogen and there are no coeval and volumetrically abundant mafic or ultramafic rocks associated with the pluton (Z.X. Li et al., 2010; Wang et al., 2010); subduction-related models, e.g. partial melting of a subducted slab and AFC process of primitive arc magma, can be precluded for the genesis of the Banshanpu pluton. Samples from the Banshanpu pluton possess low $\epsilon_{Nd}(t)$ values that are analogous to those of granite and metabasalt in the eastern Yangtze Block, which, together with their high radiogenic $^{87}Sr/^{86}Sr_i$ ratios, clearly indicate a crustal source (Fig. 10). Therefore, we tentatively consider partial melting of the mafic lower crust as the more likely regime to generate the Banshanpu pluton.

Experimental work has demonstrated that adakitic signatures can be achieved by dehydration and hydrous partial melting of a basaltic source at P-T conditions of >1.0 GPa and >650 °C (Hastie et al., 2010 and references therein). The experiments have two folds of implication. First, the residues of partial melting in the source may involve a wide range of metamorphic phases, ranging from amphibolite, garnet amphibolite, eclogite or granulite; and second, adakitic signature can be achieved at relatively low pressures (~1.0 GPa) as has been demonstrated in some studies (Johnson et al., 1997; Zellmer et al., 2012). This suggests that adakitic signature can be attained under a normal crustal thickness, and it is unnecessary to exclusively ascribe adakitic signature to an over-thickened crust.

Rocks of the Banshanpu pluton have K_2O/Na_2O ratios (0.86–1.21) significantly higher than those of typical adakites (~0.4) (Moyen, 2009). The relatively potassic composition generally reflects a K-rich mafic source (Wang et al., 2005; Xiao and Clemens, 2007). Geological investigation around the study area revealed a Late Archean to Mid-proterozoic basement consisting of greenschist to amphibolite phase tholeiitic basalt and basaltic andesite with subordinate pelite (Wu et al., 2004). Anatexis experiment for interlayered amphibolite and pelite at 10 kbar has demonstrated that a composite source will become more fertile than those with sole lithology and can give rise to more melt in dehydration-melting (Skjerlie and Patiño Douce, 1995). Despite the low-K composition of the metavolcanics, their contact with the K-rich pelite would facilitate the dehydration-melting and generate potassic melt. If the above reasoning is correct, a question arises as to what caused the adakitic signature of the Banshanpu pluton. Although both garnet and amphibole, either as fractional or residual phases, can effectively decrease the HREE and Y levels in partial melts, they cause different REE fractionation. Garnet commonly incorporates heavy REEs, while amphibole preferentially incorporates middle REEs (MREE) over heavy REEs. In the Dy/Yb vs. La/Yb diagram (Fig. 11), samples from the Banshanpu pluton exhibit a two-stage variation trend, i.e. with the increase of La/Yb ratios, their Dy/Yb ratios increase accordingly then decrease at a gentle slope. The variation trend at the first stage is coincident with the garnet vector, while the trend at the second stage

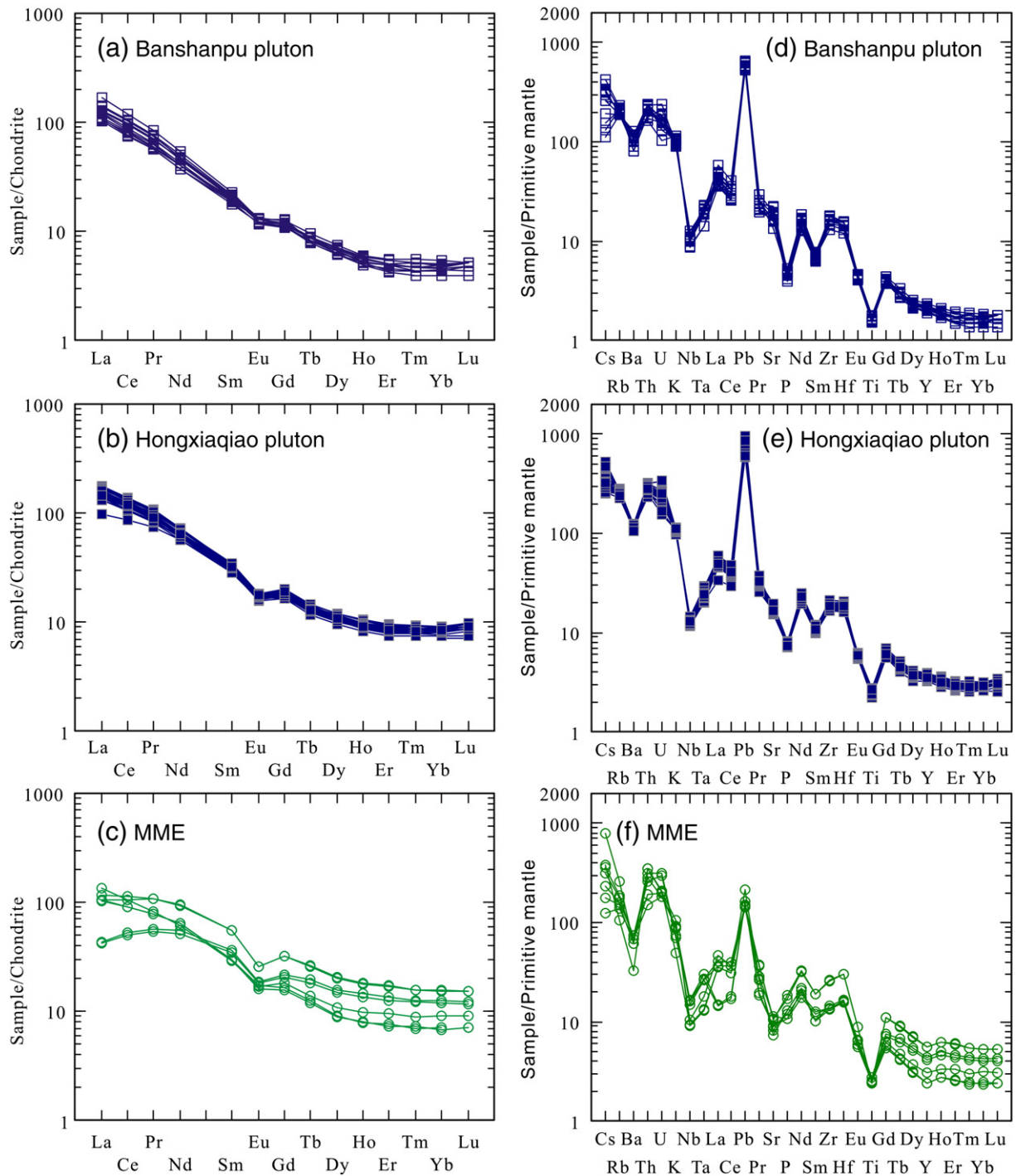


Fig. 8. Chondrite-normalized REE patterns and primitive mantle normalized multi-element diagrams for the granitoid and MME samples (Normalizing values are from Sun and McDonough, 1989).

most likely reflects the fractionation or residue of amphibole. Crystallization of amphibole can occur at both high pressure and hypobaric conditions, but amphiboles crystallized under the former condition can scavenge HREE and MREE more effectively than those in the latter case (Coldwell et al., 2011; Hastie et al., 2010; Larocque and Canil, 2010; Rodríguez et al., 2007). Because no pegmatitic or aplitic dykes occur in the Banshanpu pluton, an extreme fractionation scenario can be excluded (Clemens and Stevens, 2012). This suggests that magma of the Banshanpu pluton must be water-undersaturated and probably possessed relatively high viscosity. Therefore, it is reasonable to infer that the initially increasing and subsequently decreasing Dy/Yb ratios

with increasing La/Yb ratios most likely resulted from the residue of garnet and amphibole in the source. The source and petrogenesis of the Banshanpu pluton can be further illustrated with the Nb/Ta vs. Zr/Sm diagram (Fig. 12), which was designed to discern source nature of TTG and adakite-like rocks (Foley et al., 2002). When plotted in the diagram, all plots of the Banshanpu pluton fall into the fourth quadrant and are very close to the modeled melt of amphibolite, whereas adakitic rocks from the Tibetan Plateau exhibit much higher Nb/Ta ratios (Fig. 12). The remarkable difference between the C-type adakite in Tibet and the Banshanpu pluton implies that the crustal source of the Banshanpu pluton may not undergo significant thickening.

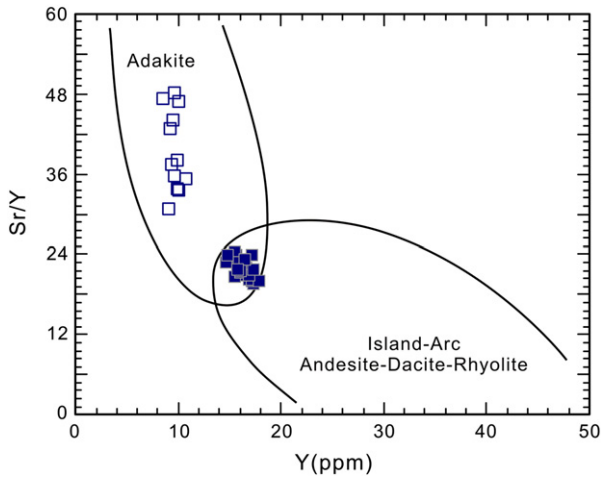


Fig. 9. Chemical discrimination diagram of Sr/Y versus Y for the Banshanpu and Hongxiaqiao plutons (after Defant and Drummond, 1993; symbols are as in Fig. 5).

5.1.2. The Hongxiaqiao pluton

Although the closely associated granitoids of the Banshanpu and Hongxiaqiao plutons possess almost identical Nd–Sr isotopic compositions, rocks from the Banshanpu and Hongxiaqiao plutons show different major and trace element compositions. Because rocks of the Hongxiaqiao pluton have lower SiO₂ but relatively higher Rb, Cs and U contents than those of the Banshanpu pluton (Table 2), they cannot readily be attributed to various degrees of fractional crystallization or partial melting of a parental magma/common source. The two plutons exhibit similar variation trend on most major oxides (Fig. 6), implying a close genetic relationship. Simultaneous emplacement and spatially adjacent occurrence strongly suggest that the two plutons may have originated from a common crustal source. A critical difference between the two plutons is that MME commonly occurs in the Hongxiaqiao pluton but is rare in the Banshanpu pluton. The occurrence of coeval MME suggests that a magma mixing regime between mantle- and crust-derived melts must have involved (Didier and Barbarin, 1991), thus it is reasonable to infer that the Hongxiaqiao and Banshanpu plutons

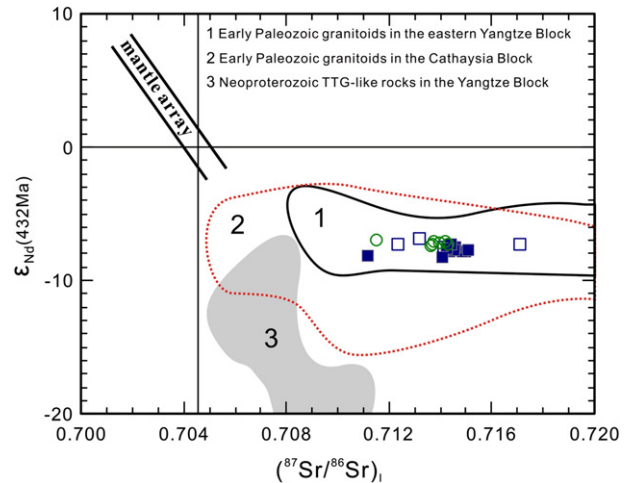


Fig. 10. Nd–Sr isotope compositions of the granitoid and MME samples (calculated at 432 Ma; symbols are as in Fig. 5). Data source: Neoproterozoic TTG-like rocks in the Yangtze Craton (Zhang et al., 2009); Early Paleozoic granites in the eastern Yangtze Block (Cheng et al., 2009a, 2009b; Zhang et al., 2012); Early Paleozoic granites in the Cathaysia Block (Bai et al., 2006; Geng et al., 2006; Z.X. Li et al., 2010; Shen et al., 2008; Y.J. Wang et al., 2011; F.R. Zhang et al., 2010; Zhang et al., 2012).

shared the same crustal source and that injection of mantle-derived magma into the Hongxiaqiao pluton made its composition deviate from that of the Banshanpu pluton. Such a mechanism can further be demonstrated by the asymptotic curve in diagrams involving two ratios of incompatible elements (Langmuir et al., 1978). In the Zr/Sm vs. Th/La diagram, all the rock samples of this study plot along a hyperbolic line, with plots of the Hongxiaqiao pluton in between those of MME and Banshanpu samples (Fig. 13). As discussed above, the precursor magma of the Banshanpu pluton rocks most likely resulted from partial melting of the lower crust, thus the Hongxiaqiao pluton was probably generated by mixing between the crustal melt with adakitic signature and a mantle-derived magma. A few sample plots deviate from the mixing lines towards lower Zr/Sm and Th/La ratios, which are probably attributed to the crystallization of zircon that contains high Zr and Th contents. Calculation based on a binary mixing model suggests that

Table 2

Sr–Nd isotopic compositions for the granitoid rocks and associated MME samples.

Sample	⁸⁷ Rb/ ⁸⁶ Sr	⁸⁷ Sr/ ⁸⁶ Sr	Error (2σ)	⁸⁷ Sr/ ⁸⁶ Sr (i)	¹⁴⁷ Sm/ ¹⁴⁴ Nd	¹⁴³ Nd/ ¹⁴⁴ Nd	Error (2σ)	εNd (t)	T _{DM} (Ma)	T _{DM2} (Ma)		
BP	YLL-3	1.4984	0.000004	0.7121	0.0917	0.511968	0.000009	−7.28	1474	1761		
	YLL-5	0.9882	0.723169	0.000004	0.7169	0.0970	0.511982	0.000009	−7.30	1523	1762	
	YLL-11	0.8315	0.719237	0.000004	0.7140	0.1034	0.511991	0.000008	−7.47	1597	1776	
HP	YLL-12	1.1875	0.720510	0.000005	0.7130	0.0895	0.511982	0.000008	−6.88	1431	1729	
	YH-1	1.2179	0.722340	0.000004	0.7146	0.1019	0.511967	0.000009	−7.88	1611	1809	
	YH-2	1.2668	0.722404	0.000003	0.7144	0.1003	0.511982	0.000008	−7.49	1567	1778	
	YH-8	1.3366	0.722313	0.000003	0.7139	0.1026	0.511946	0.000009	−8.32	1649	1845	
	YH-9	1.3680	0.719561	0.000003	0.7109	0.1068	0.511968	0.000009	−8.12	1682	1829	
	YH-13	1.3198	0.722454	0.000004	0.7141	0.0964	0.511954	0.000009	−7.82	1551	1805	
	YH-14	1.2975	0.722958	0.000004	0.7147	0.0977	0.511957	0.000009	−7.84	1565	1806	
	YH-18	1.0820	0.721741	0.000004	0.7149	0.0979	0.511972	0.000010	−7.54	1547	1782	
	YH-24	1.3610	0.722892	0.000004	0.7143	0.1005	0.511971	0.000009	−7.71	1584	1795	
	YH-26	1.2178	0.721934	0.000004	0.7142	0.0980	0.511986	0.000010	−7.28	1530	1760	
	YH-27	1.3853	0.722755	0.000004	0.7140	0.1034	0.511982	0.000009	−7.65	1610	1791	
	MME	10BG1-01	1.6246	0.723693	0.000013	0.7137	0.1402	0.512106	0.000008	−7.17	2157	1756
		10BG1-02	1.1351	0.720946	0.000020	0.7140	0.1223	0.512059	0.000008	−7.19	1813	1752
10BG1-04		1.2200	0.721272	0.000019	0.7138	0.1225	0.512063	0.000006	−7.13	1812	1747	
10BG1-06		1.7715	0.724513	0.000017	0.7136	0.1385	0.512092	0.000008	−7.45	2135	1771	
10BG2-3		1.1856	0.721471	0.000019	0.7142	0.1006	0.512002	0.000009	−7.11	1544	1747	
10BG2-4	2.7093	0.728195	0.000015	0.7115	0.0970	0.511996	0.000008	−7.03	1504	1740		
10BG2-5	1.1918	0.721625	0.000016	0.7143	0.0976	0.511982	0.000006	−7.33	1530	1765		

Notes: (1) ⁸⁷Rb/⁸⁶Sr and ¹⁴⁷Sm/¹⁴⁴Nd were calculated using whole-rock Rb, Sr, Sm and Nd contents in Table 1; (2) The errors of ⁸⁷Sr/⁸⁶Sr and ¹⁴³Nd/¹⁴⁴Nd are all 2σ; (3) εNd(t) = [(¹⁴³Nd/¹⁴⁴Nd)_s / (¹⁴³Nd/¹⁴⁴Nd)_{CHUR} − 1] × 10,000; T_{DM} = ln{[(¹⁴³Nd/¹⁴⁴Nd)_s − (¹⁴³Nd/¹⁴⁴Nd)_{DM}] / [(¹⁴⁷Sm/¹⁴⁴Nd)_s − (¹⁴⁷Sm/¹⁴⁴Nd)_{DM}]} / λ; In the calculation, (¹⁴³Nd/¹⁴⁴Nd)_{CHUR} = 0.512638, (¹⁴⁷Sm/¹⁴⁴Nd)_{CHUR} = 0.1967, (¹⁴³Nd/¹⁴⁴Nd)_{DM} = 0.51315, (¹⁴⁷Sm/¹⁴⁴Nd)_{DM} = 0.2137, λ = 0.00654 Ga^{−1} and t = 432 Ma. T_{DM2} = T_{DM} − (T_{DM} − t)(f_{cc} − f_s) / (f_{cc} − f_{DM}), where f_{cc}, f_s and f_{DM} are the f_{Sm/Nd} values of the continental crust, the sample and the depleted mantle, respectively; In this calculation, f_{cc} = −0.4 and f_{DM} = 0.08592, t = 432 Ma.

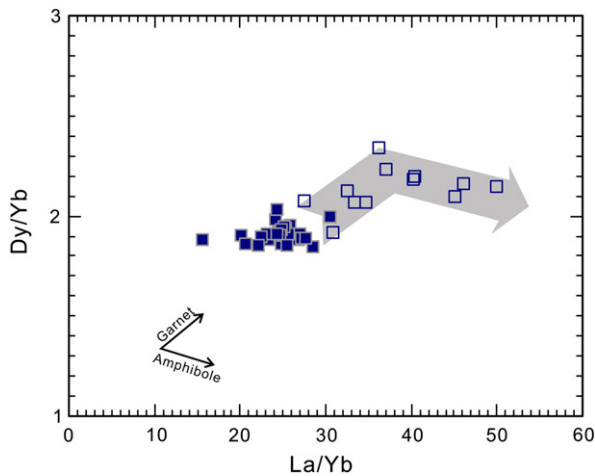


Fig. 11. La/Yb vs. Dy/Yb diagram for the granitoid and MME rocks (symbols are as in Fig. 5).

the ratio of the crustal melt to mantle-derived melt was around 6:4 (Fig. 13).

Unlike samples of the Banshanpu pluton with typical adakitic characteristics, however, samples of the Hongxiaqiao pluton possess considerably lower Sr/Y and La/Yb ratios and do not fit the criteria of adakitic rocks (Richards and Kerrich, 2007), although their Sr concentrations are equivalent to those of the Banshanpu pluton samples. We interpret this to mean that the original component of the crustal melt may be identical to the magma of the Banshanpu pluton, but that magma mixing with a mantle-derived component was responsible for the relatively low Sr/Y and La/Yb ratios of the Hongxiaqiao pluton rocks (Table 1). This inference may have important bearings on the genesis of adakitic rocks. Previous authors have concentrated on the genesis of adakitic rocks, and magma mixing has been invoked as an alternative regime to account for the formation of adakitic rocks (e.g. Guo et al., 2007). However, little attention has been paid to the possibility that melt evolution towards an adakitic composition could be aborted due to mixing with a magma that lacked a garnet signature. The mantle-derived magma, as represented by the MME samples, is characterized by relatively low Sr (<240 ppm) and high HREE (Yb ~ 2.63 ppm) contents, and their low (La/Yb)_N ratios (3–15) are consistent with a mantle source in the spinel stability field (Y.J. Wang et al., 2013; Yao et al., 2012). Involvement of such a melt from a shallow mantle source would dilute the adakitic signature

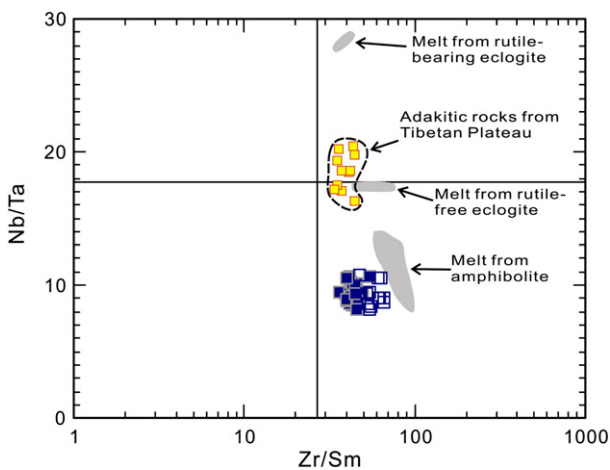


Fig. 12. Nb/Ta vs. Zr/Sm diagram for adakites and granitoid rocks of the Banshanpu and Hongxiaqiao plutons (after Foley et al., 2002; symbols are as in Fig. 5). Data of adakitic rocks by partial melting of thickened lower crust in Tibetan Plateau are from Wang et al. (2005).

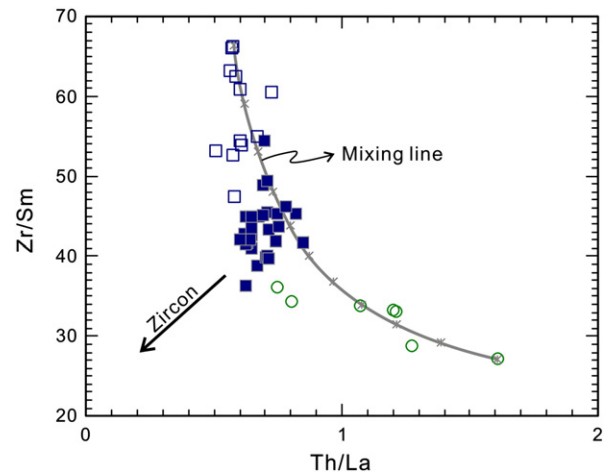


Fig. 13. Th/La vs. Zr/Sm covariant diagram for the granitoid and MMEs rocks (symbols are as in Fig. 5).

when mixed with a crustal melt and move the composition of the magma away from the adakitic field.

5.1.3. Origin of the MME

Low SiO₂ contents, high Mg# values (50–70) as well as relatively high Cr (up to 424 ppm) and Ni (up to 171 ppm) contents suggest that the MME samples most likely originated from a mantle source. The MME samples are relatively depleted in Nb–Ta (Fig. 8f), and their relatively low Nb/Ta ratios (<12.4) preclude the possibility of an origin from asthenospheric mantle. In particular, the Nd–Sr isotope compositions of the MME samples are well within the range of those of the granitoid host rocks and are distinctively different from asthenosphere-derived components. Collectively, the above evidences suggest that the MMEs most likely originated from a metasomatized lithospheric mantle.

A key issue for understanding the tectonic evolution of the Wuyi-Yunkai Orogen is the role that the mantle played during the development of the intra-continental orogeny. However, early Paleozoic mantle-derived magmatic rocks were not recognized within the Wuyi-Yunkai Orogen until recently, when high-Mg basalt and gabbroic intrusions were identified (Y.J. Wang et al., 2013; Yao et al., 2012). These mantle-derived rocks occur sporadically in the Cathaysia Block and, although variable in composition, all have been demonstrated to have an origin from metasomatized lithospheric mantle (Y.J. Wang et al., 2013; Yao et al., 2012). The MME samples have similar ages (ca. 430 Ma) and share many similarities with these high-Mg basalt and gabbroic intrusions, e.g. high Mg# values and crust-like Nd–Sr isotope compositions (Y.J. Wang et al., 2013; Yao et al., 2012), confirming their same origin from a lithospheric mantle source.

5.2. Tectonic implication for the Wuyi-Yunkai Orogen

It is now widely accepted that the Wuyi-Yunkai Orogen is an intra-continental orogen, and strong compression and intensive thrusting due to the collision between the Cathaysia and Yangtze blocks gave rise to doubly-thickened crust (Charvet et al., 2010; Faure et al., 2009; Z.X. Li et al., 2010; Wang et al., 2007; Y.J. Wang et al., 2013). Subsequent delamination and post-orogenic collapse led to the upwelling of the asthenosphere and partial melting of the lower crust to form the widespread early Paleozoic granitoids in Wuyi-Yunkai Orogen (Y.J. Wang et al., 2013; Yao et al., 2012). Although a major advance has been achieved in research of the Wuyi-Yunkai Orogen, some details of the intra-continental orogenesis still remain enigmatic.

5.2.1. Paradox of adakitic rocks

One of unexplained phenomena in the Wuyi-Yunkai Orogen is the paradox of the adakitic rocks. Lower crust-derived adakites are usually formed during collision, where crustal thickening can force the lower crust into the garnet stability field (Chung et al., 2003; Wang et al., 2005). In addition, where a thickened lithosphere was delaminated into hot asthenospheric mantle, the detached lithospheric root would melt to generate high-Mg adakitic magma (Kay and Kay, 1993; Xu et al., 2002). Field studies demonstrate that the Wuyi-Yunkai Orogen underwent significant crustal thickening due to intense thrusting (Charvet et al., 2010; Z.X. Li et al., 2010), and a crustal delamination regime was proposed to explain the wide occurrence of early Paleozoic granitoids in the SCB (Y.J. Wang et al., 2013; Yao et al., 2012). If this was the case, lower crust-derived adakitic rocks should be produced in the Wuyi-Yunkai Orogen. However, no adakitic rocks, either low-Mg or high-Mg types, have so far been reported in the Wuyi-Yunkai domains, where crustal thickening was believed to be the most intensive (Charvet et al., 2010; Faure et al., 2009; Z.X. Li et al., 2010; Wang et al., 2007, 2010). Instead, adakitic rocks (i.e. Banshanpu pluton) were produced at the northwestern margin of the Wuyi-Yunkai Orogen, far from the Wuyi-Yunkai domains.

Although pressure (i.e. crustal thickness) plays a key role in producing adakitic magma in the lower crust, temperature is also a critical factor in controlling the composition of the partial melt. Recent experimental study has revealed that the most appropriate P–T conditions for producing adakitic melt in the lower crust are 800–950 °C and 10–12.5 kb, and that higher temperature (>950–1000 °C) and pressure (>45–50 km crust) may not be favorable for the genesis of adakitic rocks (Qian and Hermann, 2013). This is because, if the temperature is too high, garnet and hornblende will be consumed to produce plagioclase and pyroxene (Getsinger et al., 2009), thus adakitic characteristics of partial melts would not be preserved.

Generally, delamination of thickened lower crust would cause extension and rapid rebound of the lithosphere (Kay and Kay, 1991; McLelland et al., 1996). Large-scale extension would lead to fast upwelling of the asthenospheric mantle, which would melt to generate mafic magma and cause underplating of the lowest part of the crust. The underplating process would further give rise to a “long lived” thermal anomaly for several tens of millions of years (Schulmann et al., 2002; Thompson, 1999). Therefore, a high temperature regime caused by the upwelling of asthenosphere, and accompanied by orogenic collapse, can best explain the widespread and synchronous none-adakitic granites in the Cathysia Block.

This hypothesis is further supported by other recent investigations. High-Mg basalt with an age of 435 Ma has been found in the Cathysia Block (Yao et al., 2012). The basalt was derived from partial melting of an ancient metasomatized sub-continental lithospheric mantle, the potential temperature of which was estimated to be higher than 1300 °C based on primary melt composition (Yao et al., 2012). Moreover, studies on a synchronous charnockite and metamorphic complex in the SW Cathysia Block revealed an intense tectonothermal event at ca. 430 Ma, characterized by high-temperature (up to 850 °C) regional metamorphism and crustal anatexis at relatively shallow crustal level (4–7 kb) (Chen et al., 2012; D. Wang et al., 2013). All these pieces of information, together with the sporadic distribution of mafic intrusions in the Wuyi-Yunkai domains (Y.J. Wang et al., 2013), indicate that the Cathysia Block experienced a more intensive tectonothermal event, with much higher temperature, than that affecting the Yangtze Block. This contrast in tectonothermal conditions may explain the differences in magmatic activity between the Cathysia and Yangtze blocks in the Early Paleozoic.

5.2.2. Two phases of orogenesis

An important issue that has puzzled researchers for a long time related to the temporal and spatial distribution of granitic intrusions in the Wuyi-Yunkai Orogen. The Early Paleozoic granites were considered

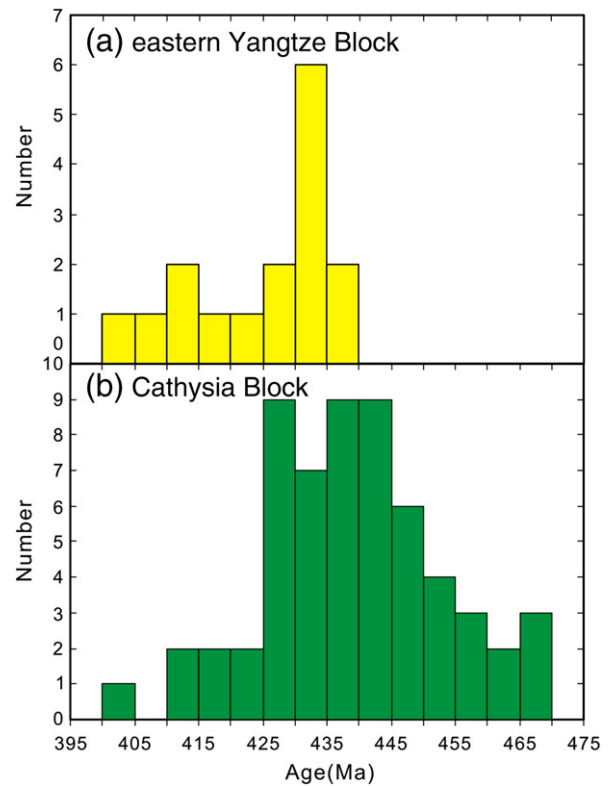


Fig. 14. Age histogram of the Early Paleozoic granitoid and migmatitic rocks in the SCB. Data source: Chen et al. (2008, 2011), Cheng et al. (2009a, 2009b), Chu et al. (2012), Geng et al. (2006), Li et al. (1989), Li (1994), J.K. Li et al. (2012), Liu et al. (2008, 2012), Peng et al. (2006), Shen et al. (2008), Sun (2006), Wang et al. (2007), Y.J. Wang et al. (2011), Wu et al. (2012), Xu et al. (2005, 2009), Yang et al. (2010), Zeng et al. (2008), A.M. Zhang et al. (2010), F.F. Zhang et al. (2010), F.R. Zhang et al. (2010), W.L. Zhang et al. (2011), L. Zhang et al. (2011), Zhao et al. (2012, 2013) and Zhu et al. (2006).

to be randomly distributed (Shu, 2012; Y.J. Wang et al., 2011, 2013). Our recent investigation of the distribution of granitic intrusions shows, however, that the Early Silurian (ca. 440 Ma) is a critical period relating to the change in distribution of the magmatic rocks. Almost all the granitic plutons with ages older than 440 Ma are confined to the eastern part of the orogen (e.g. Wuyi-Yunkai and Wugongshan domains), whereas plutons younger than 440 Ma occur throughout the Wuyi-Yunkai Orogen (Figs. 1, 14). The change in distribution of granitic plutons suggests that the Wuyi-Yunkai Orogen experienced two phases of orogenesis, with 440 Ma being the turning point.

Orogenesis was probably initiated in the Middle Ordovician (>460 Ma), when the Nanhua rift closed and a compressive regime dominated (Z.X. Li et al., 2010). During this period, intensive crustal shortening, manifested by tight folds and thrust tectonics, rapidly thickened the crust to twice its normal thickness (Charvet et al., 2010; Faure et al., 2009; Wang et al., 2012). Rapid crustal thickening resulted in intensive erosion, which gave rise to depositional rate 20 to 200 times as much as usual (Chen et al., 2010; Rong et al., 2010). Metamorphism occurred under intermediate P–T conditions, characterized by a mineral assemblage of staurolite, kyanite, garnet and biotite (BGMJRP, 1984). Anatexis was common in the Wuyi-Yunkai domains, whereas magmatism was sporadic and small in scale and dominated by granitic veins and stocks (Z.X. Li et al., 2010; Wang et al., 2012). No mafic magmatism has been identified at this time.

The second phase began in the Early Silurian (ca. 440 Ma), when tectono-magmatic processes changed significantly. Metamorphic assemblages of this phase were characterized by biotite–garnet–sillimanite–muscovite, reflecting higher temperature and lower pressure than those in the first phase (Faure et al., 2009; Zhao and Cawood, 1999). Mantle-derived mafic magma was identified for the first time in the

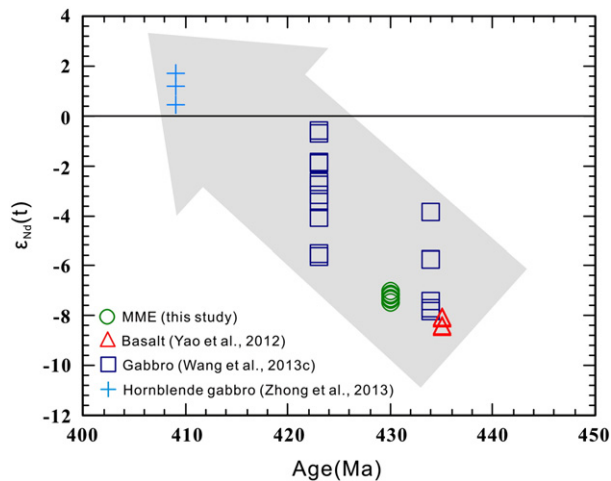


Fig. 15. ϵNd_7 vs. age diagram for the Early Paleozoic mafic rocks of the eastern SCB.

Early Silurian (ca. 435 Ma) (Yao et al., 2012), and occurred intermittently until the Early Devonian (Y.J. Wang et al., 2013; Zhong et al., 2013). These mafic magmas were mainly derived from metasomatized lithospheric mantle with a rather high potential temperature ($>1300\text{ }^\circ\text{C}$). A striking trend can be observed in the ϵNd_7 vs. age diagram (Fig. 15), i.e. with decreasing formation age, ϵNd_7 values of the mafic rocks increase significantly. This implies an increasing influence of the asthenospheric mantle, which has been attributed to the rise of the lithosphere thermal boundary during post-orogenic collapse or delamination (Y.J. Wang et al., 2013; Yao et al., 2012). Granitic intrusions were widely emplaced in both the Yangtze and Cathysia Blocks, suggesting widespread crustal melting due to the underplating of mantle-derived magmas. The presence of MMEs in the Hongxiaqiao pluton (434 Ma) suggests that the lithospheric mantle of the Cathysia and Yangtze blocks was reworked simultaneously in the Early Silurian, although the process in the Cathysia Block was more extreme.

6. Conclusions

Two closely-spaced granitoid plutons in the eastern Yangtze Block, namely the Banshanpu pluton and the Hongxiaqiao pluton have been investigated in order to provide some important constraints on the Early Paleozoic intracontinental orogeny of South China. Based on the geochronological and geochemical data as well as field observations, the following conclusions can be made:

- (1) LA-ICP-MS zircon dating indicates that the Banshanpu pluton and the Hongxiaqiao pluton formed at 432 ± 3 Ma and 434 ± 3 Ma, respectively, indicating that they were emplaced coevally in the Early Silurian.
- (2) The plutons originated from a common crustal source at the garnet stability field, which imposed typical adakitic signatures on the Banshanpu pluton. MMEs (ca. 430 Ma) in the Hongxiaqiao pluton possess less fractionated REE patterns, and their Nd–Sr isotope compositions are similar to those of the granodiorite, suggesting an origin from metasomatized spinel-phase lithospheric mantle. Rocks from the MME-bearing Hongxiaqiao pluton possess considerably lower Sr/Y and La/Yb ratios than those from the MME-absence Banshanpu pluton. It is suggested that mixing of a deep crust-derived melt with a shallow mantle-derived melt suppressed the Sr/Y and La/Yb ratios of the Hongxiaqiao pluton rocks.
- (3) An analysis of previous geochronological data from the orogen reveals two distinct pluses separated at ca. 440 Ma. The first phase is characterized by intensive crustal thickening, accompanied by anatexis and metamorphism at intermediate P–T conditions. Granitic intrusions were scattered and mostly small in scale, and no

mafic magmatism was identified in this phase. The second phase is characterized by high-T mafic magmatism, which reflects the gradually increasing influence of asthenosphere-derived melt with time. The change in magmatism and metamorphism reflects a rise of the lithosphere boundary, probably caused by delamination during post-orogenic collapse. The unusually high temperature imposed on the Cathysia Block at this time may be responsible for the scarcity of synchronous adakitic rocks in the Wuyi-Yunkai domains, where the crust was doubled in the thickness during the first phase of orogenesis.

Supplementary data to this article can be found online at <http://dx.doi.org/10.1016/j.lithos.2014.07.016>.

Acknowledgements

We thank Ms. Ying Liu and Guangqian Hu, and Mr. Xianglin Tu, for their help with the geochemical analyses. Dr. Jun Chen is thanked for providing the reference materials. The authors benefited from discussions with Professors Guochun Zhao, Wenjiao Xiao and Nengsong Chen. We are indebted to Atsushi Kamei and an anonymous reviewer, whose insightful and constructive reviews have greatly improved the paper. We thank Nelson Eby for his kind and careful editorial help. This work was co-supported by a National Natural Science Foundation of China project (41273012) and a Knowledge Innovation grant from CAS (KZCX2-YWQ08-3-6) to the corresponding author.

References

- Alonso-Perez, R., Müntener, O., Ulmer, P., 2009. Igneous garnet and amphibole fractionation in the roots of island arcs: experimental constraints on andesitic liquids. *Contributions to Mineralogy and Petrology* 157, 541–558.
- Andersen, T., 2002. Correction of common lead in U–Pb analysis that do not report ^{204}Pb . *Chemical Geology* 192, 59–79.
- Atherton, M.P., Petford, N., 1993. Generation of sodium-rich magmas from newly underplated basaltic crust. *Nature* 362, 144–146.
- Bai, D.Y., Huang, J.Z., Ma, T.Q., Wang, X.H., 2006. Geology and geochemistry of the Silurian Penggongmiao granitic pluton in the southeastern Hunan Province and its implication for tectonic setting. *Geoscience* 20, 130–140 (in Chinese with English abstract).
- BGMRHP (Bureau of Geology and Mineral Resources of Hunan Province), 1988. *Regional Geology of the Hunan Province*. Geological Publishing House, Beijing, pp. 286–507 (in Chinese with English abstract).
- BGMRJP (Bureau of Geology and Mineral Resources of Jiangxi Province), 1984. *Regional Geology of the Jiangxi Province*. Geological Publishing House, Beijing, pp. 1–921 (in Chinese with English abstract).
- Castillo, P.R., 2006. An overview of adakite petrogenesis. *Chinese Science Bulletin* 51, 258–268.
- Cawood, P.A., Tyler, I.M., 2004. Assembling and reactivating the Proterozoic Capricorn Orogen: lithotectonic elements, orogenies, and significance. *Precambrian Research* 128, 201–218.
- Chappell, B.W., Bryant, C.J., Wyborn, D., 2012. Peraluminous I-type granites. *Lithos* 153, 142–153.
- Charvet, J., Shu, L.S., Faure, M., Choulet, F., Wang, B., Lu, H.F., Le Breton, N., 2010. Structural development of the Lower Paleozoic belt of South China: genesis of an intracontinental orogen. *Journal of Asian Earth Sciences* 39, 309–330.
- Chen, Z.H., Li, J.Y., Xie, P.S., Zeng, W., Zhou, H.W., 2008. Approaching the age problem for some metamorphosed Precambrian basement rocks and Phanerozoic granitic bodies in the Wuyishan area: the application of EMP monazite age dating. *Geological Journal of China Universities* 14, 1–15 (in Chinese with English abstract).
- Chen, X., Zhang, Y.D., Fan, J.X., Cheng, J.F., Li, Q.J., 2010. Ordovician graptolite-bearing strata in southern Jiangxi with a special reference to the Kwangsian Orogeny. *Science in China Series D: Earth Sciences* 53 (1), 1602–1610.
- Chen, X.Q., Fu, J.M., Cheng, S.B., Ma, L.Y., Xu, D.M., 2011. Zircon SHRIMP U–Pb dating and mineralization significance of Yinshanling granite, northeastern Guangxi Province. *Geology and Mineral Resources of South China* 27, 85–89 (in Chinese with English abstract).
- Chen, C.H., Liu, Y.H., Lee, C.Y., Xiang, H., Zhou, H.W., 2012. Geochronology of granulite, charnockite and gneiss in the poly-metamorphosed Gaozhou Complex (Yunkai massif), South China: emphasis on the in-situ EMP monazite dating. *Lithos* 144–145, 109–129.
- Cheng, S.B., Fu, J.M., Xu, D.M., Chen, X.Q., Ma, L.Y., Wang, X.D., Pang, Y.C., 2009a. Zircon SHRIMP U–Pb dating and geochemical characteristics of Daning batholith in north-east Guangxi. *Geology of China* 36, 1278–1288 (in Chinese with English abstract).
- Cheng, S.B., Fu, J.M., Xu, D.M., Ma, L.Y., Pang, Y.C., Cao, L., 2009b. Geochemical characteristics and petrogenesis of Xuehuading granitic batholith and its enclaves, South China. *Geotectonica et Metallogenia* 33, 588–597 (in Chinese with English abstract).

- Chu, Y., Lin, W., Faure, M., Wang, Q.C., Ji, W.B., 2012. Phanerozoic tectonothermal events of the Xuefengshan Belt, central South China: implications from U–Pb age and Lu–Hf determinations of granites. *Lithos* 150, 243–255.
- Chung, S.L., Liu, D., Ji, J., Chu, M.F., Lee, H.Y., Wen, D.J., Lo, C.H., Lee, T.Y., Qian, Q., Zhang, Q., 2003. Adakites from continental collision zones: melting of thickened lower crust beneath southern Tibet. *Geology* 31, 1021–1024.
- Clemens, J.D., Stevens, G., 2012. What controls chemical variation in granitic magmas? *Lithos* 134–135, 317–329.
- Coldwell, B., Adam, J., Rushmer, T., Macpherson, C.G., 2011. Evolution of the East Philippine Arc: experimental constraints on magmatic phase relations and adakitic melt formation. *Contributions to Mineralogy and Petrology* 162, 835–848.
- Cox, K.G., Bell, J.D., Pankhurst, R.J., 1979. *The Interpretation of Igneous Rocks*. George, Allen and Unwin, London, pp. 1–450.
- Davidson, J., Turner, S., Handley, H., Macpherson, C., Dosseto, A., 2007. Amphibole “sponge” in arc crust? *Geology* 35, 787–790.
- Defant, M.J., Drummond, M.S., 1990. Derivation of some modern arc magmas by melting of young subducted lithosphere. *Nature* 347, 662–665.
- Defant, M.J., Drummond, M.S., 1993. Mount St. Helens: potential example of the partial melting of the subducted lithosphere in a volcanic arc. *Geology* 21, 547–550.
- Dessimo, M., Muntener, O., Ulmer, P., 2012. A case for hornblende dominated fractionation of arc magmas: the Chelan Complex (Washington Cascades). *Contributions to Mineralogy and Petrology* 163, 567–589.
- Didier, J., Barbarin, B., 1991. Enclaves and Granite Petrology. *Developments in Petrology* Elsevier Science Publications, Amsterdam, pp. 1–625.
- Ding, X., Zhou, X.M., Sun, T., 2005. The episodic growth of the continental crustal basement in South China: single zircon LA-ICPMS U–Pb dating of Guzhai granodiorite in Guangdong. *Geological Review* 51, 382–392 (in Chinese with English abstract).
- English, J.M., Johnston, S.T., 2004. The Laramide orogeny: what were the driving forces? *International Geology Review* 46, 833–838.
- Faure, M., Shu, L.S., Wang, B., Charvet, J., Choulet, F., Monie, P., 2009. Intracontinental subduction: a possible mechanism for the Early Palaeozoic Orogen of SE China. *Terra Nova* 21, 360–368.
- Foley, S., Tiepolo, M., Vannucci, R., 2002. Growth of early continental crust controlled by melting of amphibolite in subduction zones. *Nature* 417, 837–840.
- Garrison, J.M., Davidson, J.P., 2003. Dubious case for slab melting in the Northern volcanic zone of the Andes. *Geology* 31, 565–568.
- Geng, H.Y., Xu, X.S., O'Reilly, S.Y., Zhao, M., Sun, T., 2006. Cretaceous volcanic-intrusive magmatism in western Guangdong and its geological significance. *Science in China Series D: Earth Sciences* 36, 610–617.
- Getsinger, A., Rushmer, T., Jackson, M.D., Baker, D., 2009. Generating high Mg-numbers and chemical diversity in tonalite–trondhjemite–granodiorite (TTG) magmas during melting and melt segregation in the continental crust. *Journal of Petrology* 50, 1935–1954.
- Grove, T.L., Parman, S.W., Bowring, S.A., Price, R.C., Baker, M.B., 2002. The role of H₂O-rich fluid component in the generation of primitive basaltic andesites and andesites from the Mt Shasta region, N California. *Contributions to Mineralogy and Petrology* 251, 229–250.
- Guo, F., Nakamura, E., Fan, W.M., Kobayoshi, K., Li, C.W., 2007. Generation of Palaeocene adakitic andesites by magma mixing: Yanji Area, NE China. *Journal of Petrology* 48, 661–692.
- Hand, M., Sandiford, M., 1999. Intraplate deformation in central Australia, the link between subsidence and fault reactivation. *Tectonophysics* 305, 121–140.
- Hastie, A.R., Kerr, A.C., McDonald, I., Mitchell, S.F., Pearce, J.A., Millar, I.L., Barford, D., Mark, D.F., 2010. Geochronology, geochemistry and petrogenesis of rhyodacite lavas in eastern Jamaica: a new adakite subgroup analogous to early Archaean continental crust? *Chemical Geology* 276, 344–359.
- Hidalgo, P.J., Vogel, T.A., Rooney, T.O., Currier, R.M., Layer, P.W., 2011. Origin of silic volcanism in the Panamanian arc: evidence for a two-stage fractionation process at El Valle volcano. *Contributions to Mineralogy and Petrology* 162, 1115–1138.
- Holdsworth, R.E., Hand, M., Miller, J.A., Buick, I.S., 2001. Continental reactivation and reworking: an introduction. In: Miller, J.A., Holdsworth, R.E., Buick, I.S., Hand, M. (Eds.), *Continental Reactivation and Reworking*. Geological Society, London, Special Publications, 184, pp. 1–12.
- Hoskin, P.W.O., Kinny, P.D., Wyborn, D., Chappell, B.W., 2000. Identifying accessory mineral saturation during differentiation in granitoid magmas: an integrated approach. *Journal of Petrology* 41, 1365–1396.
- Hu, S.Q., Zhu, G., Zhang, B.L., 2010. K–Ar geochronology of the Caledonian event in the Xuefeng uplift. *Geological Review* 56, 490–500 (in Chinese with English abstract).
- Johnson, K., Barnes, C.G., Miller, C.A., 1997. Petrology, Geochemistry and Genesis of High-Al tonalite and Trondhjemites of the Cornucopia Stock, Blue Mountains Northwestern Orogen. *Journal of Petrology* 38, 1585–1611.
- Kamei, A., Miyake, Y., Owada, M., Kimura, J.I., 2009. A pseudo adakite derived from partial melting of tonalitic to granodioritic crust, Kyushu, southwest Japan arc. *Lithos* 112, 615–625.
- Kay, R.W., Kay, S.M., 1991. Creation and destruction of lower continental crust. *Geologische Rundschau* 80, 259–278.
- Kay, R.W., Kay, S.M., 1993. Delamination and delamination magmatism. *Tectonophysics* 219, 177–189.
- Kolb, M., Von Quadt, A., Peytcheva, I., Heinrich, C.A., Fowler, S.J., Cvetkovic, V., 2013. Adakite-like and normal arc magmas: distinct fractionation paths in the East Serbian segment of the Balkan–Carpathian arc. *Journal of Petrology* 54, 421–451.
- Langmuir, C.H., Vocke Jr., R.D., Hanson, G.N., Hart, S.R., 1978. A general mixing equation with applications to Icelandic basalts. *Earth and Planetary Science Letters* 37, 380–392.
- Larocque, J., Canil, D., 2010. The role of amphibolite in the evolution of arc magmas and crust: the case from the Jurassic Bonanza arc section, Vancouver Island, Canada. *Contributions to Mineralogy and Petrology* 159, 475–495.
- Le Maitre, R.W., Bateman, P., Dudek, A., Keller, J., Lameyre, J., Le Bas, M., Sabine, P., Schmid, R., Sorensen, H., Streckeisen, A., 1989. A classification of igneous rocks and glossary of terms: recommendations of the International Union of Geological Sciences Subcommittee on the Systematics of Igneous Rocks. Blackwell Oxford, pp. 1–193.
- Li, X.H., 1994. A comprehensive U–Pb, Sm–Nd, Rb–Sr and ⁴⁰Ar/³⁹Ar geochronological study on Guidong Granodiorite, southeast China: records of multiple tectonothermal events in a single pluton. *Chemical Geology* 115, 283–295.
- Li, X.H., Tatsumoto, M., Premo, W.R., Gui, X.T., 1989. Age and origin of the Tanghu granite, southeast China: results from U–Pb single zircon and Nd isotopes. *Geology* 17, 395.
- Li, X.H., Li, Z.X., Zhou, H.W., Liu, Y., Kinny, P.D., 2002. U–Pb zircon geochronology, geochemistry and Nd isotopic study of Neoproterozoic bimodal volcanic rocks in the Kangdian Rift of South China: implications for the initial rifting of Rodinia. *Precambrian Research* 113, 135–154.
- Li, X.H., Li, Z.X., Ge, W.C., Zhou, H.W., Li, W.X., Liu, Y., Wingate, M.T.D., 2003. Neoproterozoic granitoids in South China: crustal melting above a mantle plume at ca. 825 Ma? *Precambrian Research* 122, 45–83.
- Li, X.H., Liu, D.Y., Sun, M., Li, W.X., Liang, X.R., Liu, Y., 2004. Precise Sm–Nd and U–Pb isotopic dating of the Yangtze Shizhuoan polymetallic deposit and its host granite, SE China. *Geological Magazine* 141, 225–231.
- Li, W.X., Li, X.H., Li, Z.X., 2008a. Middle Neoproterozoic syn-rifting volcanic rocks in Guangfeng, South China: petrogenesis and tectonic significance. *Geological Magazine* 145, 475–489.
- Li, W.X., Li, X.H., Li, Z.X., Lou, F.S., 2008b. Obduction-type granites within the NE Jiangxi Ophiolite: implications for the final amalgamation between the Yangtze and Cathaysia Blocks. *Gondwana Research* 13, 288–301.
- Li, X.H., Li, W.X., Li, Z.X., Lo, C.H., Wang, J., Ye, M.F., Yang, Y.H., 2009a. Amalgamation between the Yangtze and Cathaysia Blocks in South China: constraints from SHRIMP U–Pb zircon ages, geochemistry and Nd–Hf isotopes of the Shuangxiwu volcanic rocks. *Precambrian Research* 174, 117–128.
- Li, X.H., Liu, Y., Li, Q.L., Guo, C.H., Chamberlain, K.R., 2009b. Precise determination of Phanerozoic zircon Pb/Pb age by multi-collector SIMS without external standardization. *Geochemistry, Geophysics, Geosystems* 10, Q04010.
- Li, Q.L., Li, X.H., Liu, Y., Tang, G.Q., Yang, J.H., Zhu, W.G., 2010a. Precise U–Pb and Pb–Pb dating of Phanerozoic baddeleyite by SIMS with oxygen flooding technique. *Journal of Analytical Atomic Spectrometry* 25, 1107–1113.
- Li, W.X., Li, X.H., Li, Z.X., 2010b. Ca. 850 Ma bimodal volcanic rocks in northeastern Jiangxi, South China: initial extension during the breakup of Rodinia? *American Journal of Science* 310, 951–980.
- Li, Z.X., Li, X.H., Wartho, J.A., Clark, C., Li, W.X., Zhang, C.L., Bao, C., 2010c. Magmatic and metamorphic events during the early Paleozoic Wuyi Yunkai orogeny, southeastern South China: new age constraints and pressure–temperature conditions. *Geological Society of America Bulletin* 122, 772–793.
- Li, H., Zhang, H., Ling, M.X., Wang, F.Y., Ding, X., Zhou, J.B., Yang, X.Y., Tu, X.L., Sun, W., 2011. Geochemical and zircon U–Pb study of the Huangmeijian A-type granite: implications for geological evolution of the Lower Yangtze River belt. *International Geology Review* 53, 499–525.
- Li, J.K., Chen, Z.Y., Chen, Z.H., Hou, K.J., Zhao, Z., 2012a. The dating and analysis of ore-forming conditions for Hanfang granite intrusions in Ganxian, Jiangxi Province. *Rock and Mineral Analysis* 31, 717–723 (in Chinese with English abstract).
- Li, X.H., Li, Z.X., He, B., Li, W.X., Li, Q.L., Gao, Y.Y., Wang, X.C., 2012b. The Early Permian active continental margin and crustal growth of the Cathaysia Block: in situ U–Pb, Lu–Hf and O isotope analyses of detrital zircons. *Chemical Geology* 328, 195–207.
- Li, X.H., Li, Z.X., Li, W.X., Wang, X.C., Gao, Y.Y., 2013a. Revisiting the “C-type adakites” of the Lower Yangtze River Belt, central eastern China: in-situ zircon Hf–O isotope and geochemical constraints. *Chemical Geology* 345, 1–15.
- Li, X.H., Tang, G.Q., Gong, B., Yang, Y.H., Hou, K.J., Hu, Z.C., Li, Q.L., Liu, Y., Li, W.X., 2013b. Qinghu zircon: a working reference for microbeam analysis of U–Pb age and Hf and O isotopes. *Chinese Science Bulletin* 58, 4647–4654.
- Li, X.H., Li, Z.X., Li, W.X., 2014. Detrital zircon U–Pb age and Hf isotope constrains on the generation and reworking of Precambrian continental crust in the Cathaysia Block, South China: a synthesis. *Gondwana Research* 25, 1202–1215.
- Liu, R., Zhang, L., Zhou, H.W., Zhong, Z.Q., Zeng, W., Xiang, H., Jin, S., Lu, X.Q., Li, C.Z., 2008. Petrogenesis of the Caledonian migmatites and related granites in northwestern Fujian Province, South China: syn-deformational crustal anatexis. *Acta Petrologica Sinica* 24, 1205–1222 (in Chinese with English abstract).
- Liu, Y.S., Gao, S., Hu, Z.C., Gao, C.G., Zong, K.Q., Wang, D.B., 2010. Continental and oceanic crust recycling-induced melt–peridotite interactions in the Trans-North China Orogen: U–Pb dating, Hf isotopes and trace elements in zircons from mantle xenoliths. *Journal of Petrology* 51, 537–571.
- Liu, S.B., Li, P., Chen, Z.Y., Chen, Z.H., Hou, K.J., Zhao, Z., Wang, C.H., 2012. Wantian Granite, Yudu of southern Jiangxi: zircon U–Pb dating and its revelation. *Rock and Mineral Analysis* 31, 724–729 (in Chinese with English abstract).
- Ludwig, K.R., 2003. *User's Manual for Isoplot/Ex Version 3.00—A Geochronology Toolkit for Microsoft Excel*. Berkeley Geochronology Center Special Publication 4, 1–70.
- Macpherson, C.G., Dreher, S.T., Thirlwall, M.F., 2006. Adakites without slab melting: high pressure differentiation of island arc magma, Mindanao, the Philippines. *Earth and Planetary Science Letters* 243, 581–593.
- Maniar, P.D., Piccoli, P.M., 1989. Tectonic discrimination of granitoids. *Geological Society of America Bulletin* 101, 635–643.
- McLelland, J., Daly, J.S., McLelland, J.M., 1996. The Grenville orogenic cycle (ca. 1350–1000 Ma): an Adirondack perspective. *Tectonophysics* 265, 1–28.

- Moyen, J.F., 2009. High Sr/Y and La/Yb ratios: the meaning of the "adakitic signature". *Lithos* 112, 556–574.
- Müntener, O., Kelemen, P.B., Grove, T.L., 2001. The role of H₂O during crystallization of primitive arc magmas under uppermost mantle conditions and genesis of igneous pyroxenites: an experimental study. *Contributions to Mineralogy and Petrology* 141, 643–658.
- Peng, S.B., Jing, Z.M., Liu, Y.H., Fu, J.M., He, L.Q., Cai, M.H., Wang, Y.B., 2006. Petrochemistry, chronology and tectonic setting of strong peraluminous anatectic granitoids in Yunkai orogenic belt, western Guangdong Province, China. *Earth Science-Journal of China University of Geosciences* 31, 110–120 (in Chinese with English abstract).
- Qian, Q., Hermann, J., 2013. Partial melting of lower crust at 10–15 kbar: constraints on adakite and TTG formation. *Contributions to Mineralogy and Petrology* 165, 1195–1224.
- Raimondo, T., Collins, A.S., Hand, M., Walker-Hallam, A., Smithies, R.H., Evins, P.M., Howard, H.M., 2010. The anatomy of a deep intracontinental orogen. *Tectonics* 29, 4024–4054.
- Richards, J.P., Kerrich, R., 2007. Special paper: adakite-like rocks: their diverse origins and questionable role in metallogenesis. *Economic Geology* 102, 537–576.
- Rodríguez, C., Selles, D., Dungan, M., Langmuir, C., Leeman, W., 2007. Adakitic dacites formed by intracrustal crystal fractionation of water-rich parent magmas at Nevado de Longav volcano (36.2 degrees S; Andean Southern Volcanic Zone, central Chile). *Journal of Petrology* 48, 2033–2061.
- Rong, J.Y., Zhan, R.B., Xu, H.G., Huang, B., Yu, G.H., 2010. Expansion of the Cathaysian Oldland through the Ordovician-Silurian transition: emerging evidence and possible dynamics. *Science in China Series D: Earth Sciences* 53, 1–17.
- Rossetti, F., Goffe, B., Monie, P., Faccenna, C., Vignaroli, G., 2004. Alpine orogenic P–T–deformation history of the Catena Costiera area and surrounding regions (Calabrian Arc, southern Italy): the nappe edifice of north Calabria revised with insights on the Tyrrhenian–Apennine system formation. *Tectonics* 23, 1560–1585.
- Sandiford, M., Hand, M., 1998. Controls on the locus of intraplate deformation in central Australia. *Earth and Planetary Science Letters* 162, 97–110.
- Schulmann, K., Schaltegger, U., Jezek, J., Thompson, A.B., Edel, J.B., 2002. Rapid burial and exhumation during orogeny: thickening and synconvergent exhumation of thermally weakened and thinned crust (Variscan orogen in Western Europe). *American Journal of Science* 302, 856–879.
- Sengör, A.M.C., Natalin, B.A., Burtman, V.S., 1993. Evolution of the Altaid tectonic collage and Palaeozoic crustal growth in Eurasia. *Nature* 364, 299–307.
- Shen, W.Z., Zhang, F.R., Shu, L.S., Wang, L.J., Xiang, L., 2008. Formation age, geochemical characteristics of the Ninggang granite body in Jiangxi Province and its tectonic significance. *Acta Petrologica Sinica* 24, 2244–2254.
- Shu, L.S., 2006. Predevonian tectonic evolution of South China: from Cathaysian Block to Caledonian period folded orogenic belt. *Geological Journal of China Universities* 12, 418–431 (in Chinese with English abstract).
- Shu, L.S., 2012. An analysis of principal features of tectonic evolution in South China Block. *Geological Bulletin of China* 31, 1035–1053 (in Chinese with English abstract).
- Shu, L.S., Faure, M., Yu, J.H., Jahn, B.M., 2011. Geochronological and geochemical features of the Cathaysia block (South China): new evidence for the Neoproterozoic breakup of Rodinia. *Precambrian Research* 187, 263–276.
- Skjerlie, K.P., Patiño Douce, A.E., 1995. Anatexis of interlayered amphibolite and pelite at 10 kbar: effect of diffusion of major components on phase relations and melt fraction. *Contributions to Mineralogy and Petrology* 122, 62–78.
- Sláma, J., Košler, J., Condon, D.J., Crowley, J.L., Gerdes, A., Hancher, J.M., Horstwood, M.S.A., Morris, G.A., Nasdala, L., Norberg, N., Schaltegger, U., Schoene, B., Tubrett, M.N., Whitehouse, M.J., 2008. Plešovice zircon—a new natural reference material for U–Pb and Hf isotopic microanalysis. *Chemical Geology* 249, 1–35.
- Stacey, J.S., Kramers, J.D., 1975. Approximation of terrestrial lead isotope evolution by a two-stage model. *Earth and Planetary Science Letters* 26, 207–221.
- Stefan, P., Stephan, K., 2006. Trace element partitioning between apatite and silicate melts. *Geochimica et Cosmochimica Acta* 70, 4513–4527.
- Sun, T., 2006. A new map showing the distribution of granites in South China and its explanatory notes. *Geological Bulletin of China* 25, 332–335 (in Chinese with English abstract).
- Sun, S.S., McDonough, W.F., 1989. Chemical and isotopic systematics of oceanic basalts: implications for mantle composition and processes. *Geological Society, London, Special Publications* 42, 313–345.
- Thompson, A.B., 1999. Some time–space relationships for crustal melting and granitic intrusion at various depths. *Geological Society, London, Special Publications* 168, 7–25.
- Tiepolo, M., Oberti, R., Vannucci, R., 2002. Trace-element incorporation in titanite: constraints from experimentally determined solid/liquid partition coefficients. *Chemical Geology* 191, 105–119.
- Wang, J., Li, Z.X., 2003. History of Neoproterozoic rift basins in South China: implications for Rodinia break-up. *Precambrian Research* 122, 141–158.
- Wang, Q., McDermott, F., Xu, J.F., Bellon, H., Zhu, Y.T., 2005. Cenozoic K-rich adakitic volcanic rocks in the Hohxil area, northern Tibet: lower-crustal melting in an intracontinental setting. *Geology* 33, 465.
- Wang, Y.J., Fan, W.M., Zhao, G.C., Ji, S.C., Peng, T.P., 2007. Zircon U–Pb geochronology of gneissic rocks in the Yunkai massif and its implications on the Caledonian event in the South China Block. *Gondwana Research* 12, 404–416.
- Wang, Y.J., Zhang, F.F., Fan, W.M., Zhang, G.W., Chen, S.Y., Cawood, P.A., Zhang, A.M., 2010. Tectonic setting of the South China Block in the early Paleozoic: resolving intracontinental and ocean closure models from detrital zircon U–Pb geochronology. *Tectonics* 29, 6020–6035.
- Wang, Y.J., Zhang, A.M., Fan, W.M., Zhao, G.C., Zhang, G.W., Zhang, Y.Z., Zhang, F.F., Li, S.Z., 2011a. Kwangsinian crustal anatexis within the eastern South China Block: geochemical, zircon U–Pb geochronological and Hf isotopic fingerprints from the gneissoid granites of Wugong and Wuyi-Yunkai Domains. *Lithos* 127, 239–260.
- Wang, Q., Li, Z.X., Chung, S.L., Wyman, D.A., Sun, Y.L., Zhao, Z.H., Zhu, Y.T., Qiu, H.N., 2011b. Late Triassic high-Mg andesite/dacite suites from northern Hohxil, North Tibet: geochronology, geochemical characteristics, petrogenetic processes and tectonic implications. *Lithos* 126, 54–67.
- Wang, Y.J., Wu, C.M., Zhang, A.M., Fan, W.M., Zhang, Y.H., Peng, T.P., Yin, C.Q., 2012. Kwangsinian and Indosinian reworking of the eastern South China Block: constraints on zircon U–Pb geochronology and metamorphism of amphibolites and granulites. *Lithos* 150, 227–242.
- Wang, D., Zheng, J.P., Ma, Q., Griffin, W.L., Zhao, H., Wong, J., 2013a. Early Paleozoic crustal anatexis in the intraplate Wuyi-Yunkai orogen, South China. *Lithos* 175–176, 124–145.
- Wang, Y.J., Fan, W.M., Zhang, G.W., Zhang, Y.H., 2013b. Phanerozoic tectonics of the South China Block: key observations and controversies. *Gondwana Research* 23, 1273–1305.
- Wang, Y.J., Zhang, A.M., Fan, W.M., Zhang, Y.H., Zhang, Y.Z., 2013c. Origin of paleosubduction-modified mantle for Silurian gabbro in the Cathaysia Block: geochronological and geochemical evidence. *Lithos* 160–161, 37–54.
- Watkins, J.M., Clemens, J.D., Treloar, P.J., 2007. Archean TTGs as sources of younger granitic magmas: melting of sodic metatonalites at 0.6–1.2 GPa. *Contributions to Mineralogy and Petrology* 154, 91–110.
- Wei, G.J., Liang, X.R., Li, X.H., Liu, Y., 2002. Precise measurement of Sr isotopic composition of liquid and solid base using (LP)MC-ICPMS. *Geochimica* 31, 295–299 (in Chinese with English abstract).
- Wiedenbeck, M., Alle, P., Corfu, F., Griffin, W.L., Meier, M., Oberli, F., Vonquadt, A., Roddick, J.C., Speigel, W., 1995. Three natural zircon standards for U–Th–Pb, Lu–Hf, trace element and REE analyses. *Geostandards Newsletter* 19, 1–23.
- Wilson, J.T., 1965. A new class of faults and their bearing on continental drift. *Nature* 207, 343–347.
- Wilson, B.M., 1989. Igneous petrogenesis a global tectonic approach. *Unwin Hyman, London*, pp. 1–300.
- Windley, B.F., 1995. The evolving continents, 3rd ed. John Wiley and Sons Chichester, pp. 1–526.
- Wu, G.Y., Li, J.D., Che, Q.J., Xiao, Q.H., Tang, X.S., Peng, H.G., 2004. Sm–Nd Dating and genesis of the Jianxichong Group metamorphic volcanic rocks in Northeast Hunan Group. *Geoscience* 18, 339–345 (in Chinese with English abstract).
- Wu, J.H., Xiang, Y.X., Huang, G.R., Liu, X.D., Liu, S., 2012. Caledonian zircon SHRIMP U–Pb age of porphyroclastic lava in northern Guangdong Province and its geological significance. *Geological Journal of China Universities* 18, 601–608 (in Chinese with English abstract).
- Xiao, L., Clemens, J.D., 2007. Origin of potassic (C-type) adakite magmas: experimental and field constraints. *Lithos* 95, 399–414.
- Xu, J.F., Shinjo, R., Defant, M.J., Wang, Q., Rapp, R.P., 2002. Origin of Mesozoic adakitic intrusive rocks in the Ningzhen area of east China: partial melting of delaminated lower continental crust? *Geology* 30, 1111–1114.
- Xu, X.S., O'Reilly, S.Y., Griffin, W.L., Deng, P., Pearson, N.J., 2005. Relict proterozoic basement in the Nanling Mountains (SE China) and its tectonothermal overprinting. *Tectonics* 24, 1652–1667.
- Xu, D.R., Chen, G.H., Xia, B., Li, P.C., He, Z.L., 2006. The Caledonian adakite-like granodiorites in Banshanpu area, eastern Hunan province, South China: petrogenesis and geological significance. *Geological Journal of China Universities* 12, 507–521 (in Chinese with English abstract).
- Xu, X.B., Zhang, Y.Q., Shu, L.S., Jia, D., Wang, R.R., Xu, H.Z., 2009. Zircon La-ICPMS U–Pb dating of the Weipu granitic pluton in southwest Fujian and the Changpu migmatite in south Jiangxi: constrains to the timing of Caledonian movement in Wuyi mountains. *Geological Review* 55, 277–285 (in Chinese with English abstract).
- Yang, D.S., Li, X.H., Li, W.X., Liang, X.Q., Long, W.G., Xiong, X.L., 2010. U–Pb and 40Ar–39Ar geochronology of the Baiyunshan gneiss (central Guangdong, south China): constraints on the timing of early Palaeozoic and Mesozoic tectonothermal events in the Wuyun (Wuyi-Yunkai) Orogen. *Geological Magazine* 147, 481–496.
- Yao, W.H., Li, Z.X., Li, W.X., Wang, X.C., Li, X.H., Yang, J.H., 2012. Post-kinematic lithospheric delamination of the Wuyi-Yunkai orogen in South China: evidence from ca. 435 Ma high-Mg basalts. *Lithos* 154, 115–129.
- Yao, W.H., Li, Z.X., Li, W.X., Li, X.H., Yang, J.H., 2014. From Rodinia to Gondwanaland: a tale of detrital zircon provenance analyses from the southern Nanhua Basin, South China. *American Journal of Science* 314, 278–313.
- Yin, A., Harrison, T.M., 2000. Geologic evolution of the Himalayan–Tibetan orogen. *Annual Review of Earth and Planetary Sciences* 28, 211–280.
- Yin, A., Nie, S., Craig, P., Harrison, T.M., Ryerson, F.J., Qian, X.L., Yang, G., 1998. Late Cenozoic tectonic evolution of the southern Chinese Tianshan. *Tectonics* 17, 1–27.
- Zellmer, G.F., Iizuka, Y., Miyoshi, M., Tamura, Y., Tatsumi, Y., 2012. Lower crustal H₂O controls on the formation of adakitic melts. *Geology* 40, 487–490.
- Zeng, W., Zhang, L., Zhou, H.W., Zhong, Z.Q., Xiang, H., 2008. Caledonian reworking of Paleoproterozoic basement in the Cathaysia Block: constraints from zircon U–Pb dating, Hf isotopes and trace elements. *Chinese Science Bulletin* 53, 895–904.
- Zhang, S.B., Zheng, Y.F., Zhao, Z.F., Wu, Y.B., Yuan, H.L., Wu, F.Y., 2009. Origin of TTG-like rocks from anatexis of ancient lower crust: geochemical evidence from Neoproterozoic granitoids in South China. *Lithos* 113, 347–368.
- Zhang, A.M., Wang, Y.J., Fan, W.M., Zhang, F.F., Zhang, Y.Z., 2010a. LA-ICPMS zircon U–Pb geochronology and Hf isotopic compositions of Caledonian granites from the Qingliu area, southwest Fujian. *Geotectonica et Metallogenia* 34, 408–418 (in Chinese with English abstract).
- Zhang, F.F., Wang, Y.J., Fan, W.M., Zhang, A.M., Zhang, Y.Z., 2010b. LA-ICPMS zircon U–Pb geochronology of late Early Paleozoic granites in eastern Hunan and western Jiangxi provinces, South China. *Geochimica* 39, 414–426 (in Chinese with English abstract).

- Zhang, F.R., Shen, W.Z., Shu, L.S., Xiang, L., 2010c. Geochemical features of granites formed at late stage of Early Paleozoic in Jiangxi Province and their geological significances. *Acta Petrologica Sinica* 26, 3456–3468 (in Chinese with English abstract).
- Zhang, F.R., Shu, L.S., Wang, D.Z., Sheng, W.Z., Yu, J.H., Xie, L., 2010d. Study on Geochronological, geochemical features and genesis of the Fufang granitic pluton in the Jiangxi Province, South China. *Geological Journal of China Universities* 16, 161–176 (in Chinese with English abstract).
- Zhang, A.M., Wang, Y.J., Fan, W.M., Zhang, F.F., Zhang, Y.Z., 2011a. LA-ICPMS zircon U–Pb geochronology and Hf isotopic composition of the Taoxi migmatite (Wuping): constraints on the formation age of the Taoxi complex and the Yu'nanian event. *Geotectonica et Metallogenia* 35, 64–72 (in Chinese with English abstract).
- Zhang, W.L., Wang, R.C., Lei, Z.H., Hua, R.M., Zhu, J.C., Lu, J.J., Xie, L., Che, X.D., Zhang, R.Q., Yao, Y., 2011b. Zircon U–Pb dating confirms existence of a Caledonian scheelite-bearing aplitic vein in the Penggongmiao granite batholith, South Hunan. *Chinese Science Bulletin* 56, 2031–2036.
- Zhang, Y., Shu, L.S., Chen, X.Y., 2011c. Geochemistry, geochronology, and petro-genesis of the early Paleozoic granitic plutons in the central-southern Jiangxi Province, China. *Science in China Series D: Earth Sciences* 54, 1492–1510.
- Zhang, F.F., Wang, Y.J., Zhang, A.M., Fan, W.M., Zhang, Y.Z., Zi, J.W., 2012. Geochronological and geochemical constraints on the petrogenesis of Middle Paleozoic (Kwangsian) massive granites in the eastern South China Block. *Lithos* 150, 188–208.
- Zhao, G.C., Cawood, P.A., 1999. Tectonothermal evolution of the Mayuan assemblage in the Cathaysia Block: implications for neoproterozoic collision-related assembly of the South China craton. *American Journal of Science* 299, 309–339.
- Zhao, Z., Chen, Z.Y., Chen, Z.H., Hou, K.J., Zhao, Z., Xu, J.X., Zhang, J.J., Zeng, Z.L., 2012. Zircon U–Pb dating, tectonic setting and ore-bearing properties evaluation of the Caledonian Yangbu Pluton in south Jiangxi. *Rock and Mineral Analysis* 31, 530–535 (in Chinese with English abstract).
- Zhao, K.D., Jiang, S.Y., Sun, T., Chen, W.F., Ling, H.F., Chen, P.R., 2013. Zircon U–Pb dating, trace element and Sr–Nd–Hf isotope geochemistry of Paleozoic granites in the Miao'ershan–Yuechengling batholith, South China: implication for petrogenesis and tectonic-magmatic evolution. *Journal of Asian Earth Sciences* 74, 244–264.
- Zheng, Y.F., Wu, R.X., Wu, Y.B., Zhang, S.B., Yuan, H.L., Wu, F.Y., 2008. Rift melting of juvenile arc-derived crust: geochemical evidence from Neoproterozoic volcanic and granitic rocks in the Jiangnan Orogen, South China. *Precambrian Research* 163, 351–383.
- Zhong, Y.F., Ma, C.Q., Zhang, C., Wang, S.M., She, Z.B., Liu, L., Xu, H.J., 2013. Zircon U–Pb age, Hf isotopic compositions and geochemistry of the Silurian Fengdingshan I-type granite Pluton and Taoyuan mafic-felsic Complex at the southeastern margin of the Yangtze Block. *Journal of Asian Earth Sciences* 74, 11–24.
- Zhu, J.C., Zhang, P.H., Xie, C.F., Zhang, H., Yang, C., 2006. Zircon U–Pb age framework of Huashan-Guposhan intrusive belt, western part of Nanling Range, and its geological significance. *Acta Petrologica Sinica* 22, 2270–2278 (in Chinese with English abstract).